TITLE

Regulation of mitophagy by the NSL complex underlies genetic risk for Parkinson's disease at Chr16q11.2 and on the MAPT H1 allele

AUTHOR INFORMATION

Marc P.M. Soutar[1,*], Daniela Melandri[1,*], Emily Annuario[1,*], Amy E. Monaghan[2,3], Natalie J. Welsh[4], Karishma D'Sa[1,5], Sebastian Guelfi[1], David Zhang[1], Alan Pittman[6], Daniah Trabzuni[1], Kylie S. Pan[1], Demis A. Kia[1], Magda Bictash[2,3], Sonia Gandhi[1,7], Henry Houlden[1], Mark R. Cookson[8], Nicholas W Wood[1], Andrew B. Singleton[8], John Hardy[1,3], Paul J. Whiting[2,3], Cornelis Blauwendraat[8], Alexander J. Whitworth[4], Claudia Manzoni[1,9], Mina Ryten[1,†], Patrick A. Lewis[1,9,†] & Hélène Plun-Favreau[1,†,‡]

[1] UCL Queen Square Institute of Neurology, London, UK
[2] UCL Alzheimer's Research UK, Drug Discovery Institute, London, UK
[3] UCL Dementia Research Institute, London, UK
[4] MRC Mitochondrial Biology Unit, University of Cambridge, Cambridge, UK
[5] KCL, London, SE1 1UL, UK
[6] St Georges University, London, UK
[7] Francis Crick Institute, London, UK
[8] Laboratory of Neurogenetics, National Institute on Aging, National Institutes of Health, Bethesda, MD, USA
[9] School of Pharmacy, University of Reading, Reading, UK

* and † these authors contributed equally to the work
‡ corresponding author

RUNNING TITLE

New mitophagy Parkinson's risk genes

ABSTRACT

Parkinson's disease (PD) is a common incurable neurodegenerative disease. The identification of genetic variants via genome-wide association studies (GWAS) has considerably advanced our understanding of the PD genetic risk. Understanding the functional significance of the risk loci is now a critical step towards translating these genetic advances into an enhanced biological understanding of the disease. Impaired mitophagy is a key causative pathway in familial PD, but its relevance to idiopathic PD is unclear. We used a mitophagy screening assay to evaluate the functional significance of risk genes identified through GWAS. We identified two new regulators of PINK1-mitophagy, KAT8 and KANSL1, previously shown to modulate lysine acetylation. These findings establish PINK1-mitophagy as a contributing factor to idiopathic PD. *KANSL1* is located on chromosome 17q21 where the risk associated gene has long been considered to be *MAPT*. Our data provide evidence that this assignment is likely to be incorrect and that variability at *KANSL1* underpins this association. Finally, these results enrich our understanding of physiological events regulating mitophagy and establish a novel pathway for drug targeting in neurodegeneration.

KEY WORDS

GWAS / KANSL1 / KAT8 / mitophagy / Parkinson's disease

INTRODUCTION

Parkinson's disease (PD) is the most common movement disorder of old age and afflicts more than 125,000 in the UK [1]. Temporary symptomatic relief remains the cornerstone of current treatments, with no disease-modifying therapies yet available [2]. Until recently, the genetic basis for PD was limited to family-based linkage studies, favouring the identification of rare Mendelian genes of high penetrance and effect. However, genome-wide association studies (GWAS) have identified large numbers of common genetic variants linked to increased risk of developing the disease [3,4]. While these genetic discoveries have led to a rapid improvement in our understanding of the genetic architecture of PD [5], they have resulted in two major challenges for the research community. First, conclusively identifying the causal gene(s) for a given risk locus, and secondly dissecting their contribution to disease pathogenesis. Addressing these challenges is critical for moving beyond genetic insights to developing new disease-modifying strategies for PD.

Previous functional analyses of *PINK1* and *PRKN*, two genes associated with autosomal recessive PD, have highlighted the selective degradation of damaged mitochondria (mitophagy) as a key contributor to disease pathogenesis. In mammalian cells, the mitochondrial kinase PINK1 selectively accumulates at the surface of damaged mitochondria, where it phosphorylates ubiquitin, leading to the recruitment of the E3 ubiquitin ligase Parkin. The recruitment of autophagy receptors leads to the engulfment of damaged mitochondria in autophagosomes, and ultimately fusion with lysosomes [6–11]. It has subsequently become clear that other PD-associated Mendelian genes, such as *FBXO7*, *DJ-1* and *VPS35* [12], are implicated in the regulation of PINK1-mediated mitochondrial quality control. Based upon these data, we hypothesised that PD-GWAS candidate genes may also be involved in this process, providing a mechanistic link between these genes and the aetiology of idiopathic PD. In order to test that hypothesis, we used functional genomics to prioritise candidate genes on the PD GWAS loci, and we developed a biological screening assay as a tool to identify genes that regulate PINK1-mitophagy, and as such, are very likely to be genes that increase the risk of developing PD.

In this study, we show that *KAT8* and *KANSL1*, two genes that were previously shown to be part of the same lysine acetylase complex partially located at the mitochondria [13], are two new important regulators of PINK1-mediated mitochondrial quality control. These findings establish mitophagy as a contributing factor to idiopathic PD and provide a proof of principle for the value of screening approaches to identify causative genes in GWAS loci. Finally, these results suggest lysine acetylation as a potential new avenue for mitophagy modulation and therapeutic intervention.

RESULTS

82 Genomic analyses of PD have identified over 80 loci associated with an increased lifetime
83 risk for disease. In contrast to Mendelian PD genes, however, the assignment of a causative gene to
84 a risk locus is often challenging. In order to identify new risk genes for PD, we undertook a triage of
85 PD GWAS candidate genes using a combination of methods: i) Colocalization (Coloc) and
86 transcriptome-wide association analysis (TWAS) [14] using expression quantitative trait loci (eQTLs)
87 information derived from Braineac [15], GTEx and CommonMind resources [16,17] to link PD risk variants
88 with specific genes, ii) weighted protein-protein interaction (PPI) network analysis (WPPINA) [18]
89 based on Mendelian genes associated with PD, and iii) the prioritised gene set as described in PD-
90 GWAS [3,19]. 31 open reading frames (ORFs) were nominated as putatively causal for associations at PD
91 risk loci. 55% of these genes were prioritised through multiple techniques (Fig. 1a), with three out of
92 31 genes (*KAT8, CTSB* and *NCKIPSD*) identified through all three prioritization methods (Fig. 1b, c).
93 The 31 genes, together with 7 PD Mendelian genes and lysosomal storage disorder genes, previously
94 shown to be enriched for rare, likely damaging variants in PD [20], were then taken forward for
95 functional analysis (Supplementary Table 1).
96 Based upon extensive data implicating impaired mitophagy in the aetiology of familial PD [7],
97 we hypothesized that additional PD-GWAS candidate genes, involved in the most common,
98 idiopathic form of the disease, may play a role in this process. In order to test whether the 38
99 prioritised genes have a role in PINK1-mitophagy, we developed and optimized a high content
100 screening (HCS) assay for phosphorylation of ubiquitin at serine 65 (pUb(Ser65)), a PINK1-dependent
101 mitophagy marker [21], following mitochondrial depolarization (Extended Data Fig. 1a and 2). The 38
102 prioritised genes were individually knocked down (KD) using siRNA in Parkin over-expressing (POE)-
103 SHSY5Y human neuroblastoma cells. Increased mitochondrial clearance following mitochondrial
104 depolarization induced by treatment with 10 µM of oligomycin/antimycin A (O/A) was validated as
105 an endpoint for mitophagy (Extended Data Fig. 1b). Over 97% of the pUb(Ser65) signal colocalised
106 with the TOM20 mitochondrial marker in O/A treated cells (Extended Data Fig. 1c, d). siRNA KD
107 efficiency was validated using both a pool of *PINK1* siRNA, which decreased O/A induced pUb(Ser65)
108 and subsequent TOM20 degradation (Extended Data Fig. 1e-g) without decreasing cell viability
109 (Extended Data Fig. 3a, b), and a pool of Polo-like kinase 1 (PLK-1) siRNA that decreased cell viability
110 by apoptosis (Extended Data Fig. 3a, b). The siRNA pools for the 38 candidate genes, together with
111 controls, were screened in duplicate on each plate, across three replicate plates per run. Hits were
112 identified as those wells where O/A-induced pUb(Ser65) was decreased or increased at greater than
113 two standard deviations from the mean of the scramble (SCR) negative control siRNA.
114 *KAT8* was selected based on reproducible downregulation of O/A-induced PINK1-dependent
115 pUb(Ser65) across all three replicates (Fig. 2a and Extended Data Fig. 1h), without affecting cell

116 viability (Extended Data Fig. 3c). Notably, *KAT8* was selected as a candidate gene on the basis of all
117 three prioritization criteria – namely, proximity of the lead SNP to an ORF, colocalization of a brain-
118 derived eQTL signal with a PD GWAS association signal (Extended Data Fig. 4) and evidence of PPI
119 with a known PD gene (Fig. 1). Furthermore, we find that colocalization and Transcriptome-wide
120 Association Study (TWAS) [22] analyses at this locus are consistent with the KD models in the HCS assay
121 (Supplementary Tables 2 and 3) [17]. Both methods predict that the risk allele operates by reducing
122 *KAT8* expression in PD cases versus controls. The effect of KAT8 KD on pUb(Ser65) was further
123 validated in POE SHSY5Y cells treated with either 1 or 10 µM O/A, using both immunofluorescence
124 (IF) and immunoblotting (IB) (Fig. 3a-d and Extended Data Fig. 5a-e). In order to assess whether
125 other lysine acetyltransferases (KATs) could regulate PINK1-dependent mitophagy, the pUb(Ser65)
126 screen was repeated in POE SHSY5Y cells silenced for 22 other KATs [23,24]. Only *KAT8* KD led to a
127 decreased pUb(Ser65) signal, emphasising the specificity of the KAT8 KD effect on pUb(Ser65) (Fig.
128 3e and Supplementary Table 4).
129 These functional data complement and support the Omic prioritization of *KAT8* as a
130 causative gene candidate for the chromosome 16q11.2 PD associated locus (Fig. 2b). To gain further
131 insight into a possible role for KAT8 in the aetiology of PD, we explored the known functional
132 interactions of this protein. KAT8 has previously been shown to partially localise to mitochondria as
133 part of the NSL complex together with KANSL1, KANSL2, KANSL3, and MCRS1 [13] (Fig. 4a). To test
134 whether other components of the NSL complex also modulate mitophagy, the pUb(Ser65) screen
135 was repeated in POE SHSY5Y cells silenced for each of the nine NSL components (HCFC1, KANSL1,
136 KANSL2, KANSL3, KAT8, MCRS1, OGT, PHF20, WDR5) (Fig. 4a). Notably, reduction of KANSL1,
137 KANSL2, KANSL3, MCRS1 and KAT8 expression led to decreased pUb(Ser65) after 1.5 or 3 h O/A
138 treatment (Fig. 4b,c). Strikingly, *KANSL1* is another PD GWAS candidate gene [3]. The effect of KANSL1
139 KD on pUb(Ser65) was further validated in POE SHSY5Y cells treated with 1 µM O/A, using both IF
140 and IB (Fig. 5a-d). A time course experiment was designed to compare the effect of KAT8 and
141 KANSL1 KD on PINK1-dependent pUb(Ser65) (Fig. 6a,b and Supplementary table 5) and subsequent
142 mitophagy (Fig. 7a,b). While individual KD of either KANSL1 or KAT8 affect phosphorylation of
143 ubiquitin, KANSL1 KD decreased pUb(Ser65) and mitophagy, as assessed by measuring the puncta of
144 the mitochondrial marker PMPCB [25], more efficiently than KAT8 KD (Fig. 6a,b and Fig. 7a,b). To
145 assess the role of KAT8/KANSL1 in neuronal function and survival *in vivo*, we used *Drosophila* as a
146 simple model system. Notably, the NSL complex was originally discovered in *Drosophila* through the
147 homologs of *KAT8* and *KANSL1* (*mof* and *nsl1*, respectively), but null mutants for these genes are
148 associated with developmental lethal owing to profound transcriptional remodelling during
149 development [26]. Therefore, we utilised inducible transgenic RNAi strains to target the KD of *mof* and

150 *nsl1* specifically in neuronal tissues. Using behavioural assays as a sensitive readout of neuronal
151 function we found that pan-neuronal KD of *mof* or *nsl1* caused progressive loss of motor (climbing)
152 ability (Extended data Fig. 6a, b), and also significantly shortened lifespan (Extended data Fig. 6c, d).
153 Interestingly, loss of *nsl1* had a notably stronger effect than loss of *mof*. Consistent with this, KD of
154 *nsl1* but not *mof*, in either all neurons or only in dopaminergic (DA) neurons, caused the loss of DA
155 neurons (Extended data Fig. 6e, f).
156 *KANSL1* is located within the extensively studied inversion polymorphism on chromosome
157 17q21 (Extended data Fig. 7a, b), which also contains *MAPT* - a gene frequently postulated to drive
158 PD risk at this locus [27]. While the majority of individuals inherit this region in the direct orientation,
159 up to 25% of individuals of European descent have a ∼1mb sequence in the opposite orientation
160 [28,29], inducing a larger ∼1.3–1.6 Mb region of linkage disequilibrium (LD). Since this inversion
161 polymorphism precludes recombination over a region of ∼1.3–1.6 Mb, haplotype-specific
162 polymorphisms have arisen resulting in the generation of two major haplotype clades, termed H1
163 (common haplotype) and H2 (inversion carriers), previously strongly linked to neurodegenerative
164 disease [30,31]. Due to high LD, the genetics of this region have been hard to dissect, and robust eQTL
165 analyses have been challenging due to the issue of polymorphisms within probe sequences in
166 microarray-based analyses or mapping biases in RNA-seq-based analyses. Several variants
167 (rs34579536, rs35833914 and rs34043286) are in high LD with the H1/H2 haplotype and are located
168 within *KANSL1* (Fig. 8a,b), which could directly impact on KANSL1 protein function. In particular, one
169 of the missense variants is a serine to proline change in KANSL1 protein sequence (S718P), and
170 would therefore be predicted to alter the gross secondary structure of the KANSL1 protein (Fig. 8b).
171 Furthermore, we used allele-specific expression (ASE) analysis to explore the possibility that PD risk
172 might be mediated at this locus through an effect on *KANSL1* expression. Using RNA sequencing data
173 generated from 84 brain samples (substantia nigra n=35; putamen n=49), for which we had access to
174 whole exome sequencing and SNP genotyping data thus enabling mapping to personalised genomes
175 [32], we quantified the variation in expression between the H1 and H2 haplotypes (Supplementary
176 Table 6). While we identified ASE sites within *MAPT* (Extended Data Fig. 8 and Supplementary Table
177 7), we also identified 4 sites of allele-specific expression in *KANSL1* (Fig. 8a), suggesting that the high
178 PD risk H1 allele is associated with lower *KANSL1* expression, consistent with our functional
179 assessment. Interestingly, sequence analysis of the human *KANSL1* haplotype revealed that the high
180 risk H1 haplotype is the more recent "mutant" specific to *Homo sapiens*, and that other primates
181 and mammals share the rarer non-risk ancestral H2 haplotype (Figure 8b).
182 To assess the specificity of the KANSL1 KD effect on PINK1-mitophagy, 32 open reading
183 frames in linkage disequilibrium on the H1 haplotype at the 17q21 locus (Extended data Fig. 7a, b

184 and Supplementary Table 8) were knocked down individually and their effect on pUb(Ser65) was
185 assessed. While the effect of *KANSL1* KD on pUb(Ser65) was confirmed, neither the KD of *MAPT*, nor
186 the KD of each of the other 30 genes on this locus, led to a decreased in the pUb(Ser65) signal (Fig.
187 9). These data confirm the selectivity of our mitophagy screening assay and suggest that KANSL1 is
188 likely to be a key PD risk gene at the 17q21 locus.
189
190 **DISCUSSION**
191 Since the first PD GWAS study was performed in 2006 [33] GWAS have identified about 90
192 independent loci for PD [4]. However, translating GWAS findings into a new molecular understanding of PD-
193 associated pathways and new therapeutic targets has remained a major challenge for the scientific
194 community. In order to screen for PD GWAS candidate genes that play a role in PINK1-mitophagy, and thus
195 are likely to be genuine risk genes for PD, we have set up and optimised a HCS for pUb(Ser65), a marker of
196 PINK1-dependent mitophagy, a key pathway in PD pathogenesis. This approach allowed the successful
197 identification of two new genes associated with increased PD risk, that play a role in mitophagy.
198 Interestingly, these two genes were previously shown to be part of the same complex, the NSL complex.
199 This study demonstrates the substantial potential of functional screens to exploit genetic data by
200 providing orthogonal information that can confidently identify new risk genes. This is particularly
201 important in genomic regions with uniformly high linkage disequilibrium, such as the 17q21 inversion
202 region which includes 32 ORFs of which many are highly expressed in brain and where existing fine-
203 mapping and functional genomic analyses have been inconclusive. Interestingly, while *MAPT* has long been
204 considered the risk associated gene at this locus, this has recently been questioned by Dong and
205 colleagues, who also raised the significance of KANSL1 in driving PD risk at the locus [34]. Furthermore,
206 functional screening can simultaneously provide mechanistic insights as exemplified in this case by the
207 novel insights we provide into the molecular events regulating mitochondrial quality control and which
208 support a role for mitophagy as a contributing factor to sporadic PD. While our data demonstrate an
209 unequivocal role for KAT8 and KANSL1 in PINK1-dependent ubiquitin phosphorylation and subsequent
210 mitophagy, the precise mechanism of regulation remains to be determined. Our results identify KAT8 and
211 KANSL1 as modifiers of PINK1-dependent pUb(Ser65), suggesting that they may be regulating PINK1 kinase
212 activity. It will be important to determine whether phosphorylation of other PINK1 substrates, such as
213 Parkin and Rab8A [9,35], are modulated by KAT8 and KANSL1. The KAT8 and KANSL1-containing NSL complex
214 functions to promote histone acetylation and as such, is a master regulator of transcription [36]. Therefore,
215 another possibility is that KAT8/KANSL1 may regulate PINK1 transcription, and subsequent translation.
216 Interestingly, depletion of KAT8/KANSL1 was shown to cause significant downregulation of mitochondrial
217 DNA transcription and translation, and ultimately impaired mitochondrial respiration [13]. Thus, it is also

218 possible that KAT8/KANSL1-dependent modulation of mitochondrial DNA indirectly regulates PINK1
219 mitochondrial accumulation and subsequent mitophagy. Finally, an intriguing possibility is that the
220 KAT8/KANSL1 complex directly acetylates ubiquitin, which has previously been shown to be acetylated on
221 six out of its seven lysines (K6, K11, K27, K33, K48, K63) [37]. It has been proposed that the KAT8/KANSL1
222 complex has targets in the mitochondria other than the mitochondrial DNA [13]. Further experiments are
223 required to determine whether KAT8, which has been shown to partially localise at the mitochondrial
224 outer membrane, where ubiquitin is phosphorylated [13], may contribute to ubiquitin acetylation.
225 Important genetic discoveries in PD, in particular, the identification of the *PINK1* [38] and *PRKN* genes
226 [39], opened the field of selective mitophagy [7]. However, there is still a clear need for a better molecular
227 understanding of mitochondrial quality control. Here we provide new insights into the mechanism by
228 identifying two new molecular players, KAT8 and KANSL1. These new regulators of mitophagy provide the
229 first direct evidence for a role of the PINK1-mitophagy pathway in idiopathic PD and the convergence
230 between familial and idiopathic pathways in disease. Taken together, these findings open a novel avenue
231 for the therapeutic modulation of mitophagy in PD, with potential implications across drug discovery in
232 frontotemporal dementia and Alzheimer's disease, where mitophagy also plays an important role in
233 disease pathogenesis [40].
234

235 **METHODS**

236

237 **Reagents**

238 Oligomycin (mitochondrial complex V inhibitor) was purchased from Cayman Chemicals (11341) and
239 from Sigma-Aldrich (O4876), and antimycin A (mitochondrial complex III inhibitor) was purchased
240 from Sigma-Aldrich (A8674). All siRNAs were purchased as pre-designed siGENOME SMARTpools
241 from Dharmacon: non-targeting (D-001206-13), PINK1 (M-004030-02), PLK1 (L-003290-00), KIF-11
242 (L-003317-00), KAT8 (M-014800-00), KANSL1 (M-031748-00), KANSL2 (M-020816-01), KANSL3 (M-
243 016928-01), HCFC1 (M-019953-01), MCRS1 (M-018557-00), OGT (M-019111-00), PHF20 (M-015234-
244 02), WDR5 (M-013383-01). The following antibodies were used for immunocytochemistry: mouse
245 anti TOM20 (Santa Cruz, sc-17764, 1:1000), rabbit anti phospho-ubiquitin (Ser65) (Cell Signaling,
246 37642, 1:1000), rabbit anti PMPCB (Proteintech 16064-1-AP, 1:1000), AlexaFluor 488 goat anti rabbit
247 (Invitrogen, A11008, 1:2000), AlexaFluor 568 goat anti mouse (Invitrogen, A11004, 1:2000). The
248 following antibodies were used for immunoblotting: mouse anti TIM23 (BD Biosciences, 611223,
249 1:1000), rabbit anti phospho-ubiquitin (Ser65) (Merck Millipore, ABS1513-I, 1:1000), mouse anti
250 GAPDH (Abcam, ab110305, 1:1000), rabbit anti KAT8 (Abcam, ab200600, 1:1000), IRDye 680LT
251 donkey anti mouse (LI-COR Biosciences, 925-68022, 1:20000), IRDye 800CW donkey anti rabbit (LI-
252 COR Biosciences, 925-32213, 1:20000).

253

254 **Selection of genes for High Content Screening**

255 Candidates for High Content Screening were selected based on i) WPPINA; ii) complex prioritization;
256 and, iii) coloc analysis. WPPINA analysis is reported in [18] where the 2014 PD GWAS [19] was analysed;
257 candidate genes where selected among those prioritised and with an LD r2 ≥ 0.8. The same pipeline
258 has then been additionally applied to the 2017 PD GWAS [3] to update the list of candidate genes.
259 Briefly, a protein-protein interaction network has been created based on the Mendelian genes for
260 PD (seeds) using data from databases within the IMEx consortium. The network has been
261 topologically analysed to extract the core network (i.e. the most interconnected part of the
262 network). The core network contains the proteins/genes that can connect >60% of the initial seeds
263 and are therefore considered relevant for sustaining communal processes and pathways, shared by
264 the seeds. These processes have been evaluated by Gene Ontology Biological Processes enrichment
265 analysis. The top SNPs of the 2017 PD GWAS have been used to extract open reading frames (ORFs)
266 in cis-haplotypes defined by LD r2 ≥ 0.8 (analysis performed in October 2017) [3]. These ORFs have
267 been matched to the core network to identify overlapping proteins/genes in relevant/shared
268 pathways. Results of complex prioritization (neurocentric prioritization strategy) were gathered from

269 [3] where this strategy was applied to the 2017 PD GWAS [3]. The coloc analysis was performed as
270 reported in [17], posterior probabilities for the hypothesis that both traits, the regulation of expression
271 of a given gene and the risk for PD share a causal variant (PPH4), were calculated for each gene, and
272 genes with PPH4 ≥ 0.75 were considered to have strong evidence for colocalization. Summary
273 statistics were obtained from the most recent PD GWAS [4] and were used for regional association
274 plotting using LocusZoom [41].
275
276 **Cell Culture and siRNA transfection**
277 POE SH-SY5Y cells are a kind gift from H. Ardley [42]. Cells were cultured in Dulbecco's Modified Eagle
278 (DMEM, Gibco, 11995-065) and supplemented with 10% heat-inactivated foetal bovine serum (FBS,
279 Gibco) in a humidified chamber at 37 °C with 5% CO_2. For siRNA transfection, cells were transfected
280 using DharmaFECT1 transfection reagent (Dharmacon, T-2001-03) according to the manufacturer's
281 instructions (for concentrations of siRNA, see sections below).
282
283 **ASEs**
284 Sites of ASE were identified as described by Guelfi and colleagues [32] by mapping RNA-seq data to
285 personalised genomes, an approach specifically chosen because it aims to minimise the impact of
286 mapping biases. RNA-seq data generated from 49 putamen and 35 substantia nigra tissue samples
287 from the UK Brain Expression Consortium was used for this analysis. All samples were obtained from
288 neuropathologically normal individuals of European descent and sites with greater than 15 reads in a
289 sample were tested for ASE. Only sites present in non-overlapping genes were considered and data
290 from both the tissues were considered together to increase power. Sites with minimum FDR < 5%
291 across samples were marked as ASE sites. Plots were generated using Gviz3, with gene and
292 transcript details obtained from Ensembl v92.
293
294 **High Content siRNA Screen**
295 ***Cell plating and siRNA transfection***
296 siRNA was dispensed into Geltrex-coated 96-well CellCarrier Ultra plates (Perkin Elmer) at a final
297 concentration of 30 nM using the Echo 555 acoustic liquid handler (Labcyte). For each well, 25 µl of
298 DMEM containing 4.8 µl/ml of DharmaFECT1 transfection reagent was added and incubated for 30
299 min before POE SH-SY5Y cells were seeded using the CyBio SELMA (Analytik Jena) at 15,000 cells per
300 well, 100 µl per well in DMEM + 10% FBS. Cells were incubated for 72 h before treatment with 10
301 µM oligomycin/10 µM antimycin for 3 h to induce mitophagy.
302 ***IF and Image Capture and Analysis***

303 Cells were fixed with 4% PFA (Sigma-Aldrich, F8775), then blocked and permeabilised with 10% FBS,
304 0.25% Triton X-100 in PBS for 1 h, before immunostaining with pUb(Ser65) and TOM20 primary
305 antibodies (in 10% FBS/PBS) for 2 h at room temperature. After 3x PBS washes, AlexaFluor 568 anti-
306 mouse and 488 anti-rabbit secondary antibodies and Hoechst 33342 (Thermo Scientific, 62249) were
307 added (in 10% FBS/PBS, 1:2000 dilution for all) and incubated for 1 h at room temperature.
308 Following a final 3x PBS washes, plates were imaged using the Opera Phenix (Perkin Elmer). 5x fields
309 of view and 4x 1 µm Z-planes were acquired per well, using the 40X water objective, NA1.1. Images
310 were analysed in an automated way using the Columbus 2.8 analysis system (Perkin Elmer) to
311 measure the integrated intensity of pUb(Ser65) within the whole cell (see Extended Data Fig. 1 and 2
312 for image analysis workflow and parameters).

313 ***Screen quality control, data processing and candidate selection***

314 Screen plates were quality controlled based on the efficacy of the PINK1 siRNA control and O/A
315 treatment window (minimum 3-fold). Data were checked for edge effects using Dotmatics Vortex
316 visualization software. Raw data was quality controlled using robust Z prime > 0.5. Data were
317 processed using Python for Z score calculation before visualization in Dotmatics Vortex. Candidates
318 were considered a hit where Z score was ≥ 2 or ≤ -2, and where replication of efficacy was seen both
319 within and across plates.

320 ***siRNA libraries***

321 The siRNA libraries were purchased from Dharmacon as an ON-TARGETplus SMARTpool Cherry-pick
322 siRNA library, 0.25 nmol in a 384-well plate. siRNAs were resuspended in RNase-free water for a final
323 concentration of 20 µM. SCR, PINK1 and PLK1 or KIF11 controls were added to the 384-well plate at
324 a concentration of 20 µM before dispensing into barcoded assay-ready plates.

325

326 **Mitochondrial enrichment and Western blotting**

327 POE SH-SY5Y cells were transfected with 100 nM siRNA and incubated for 72 h. Cell lysates were
328 fractionated into cytoplasmic and mitochondria-enriched samples, and run on SDS-PAGE before IB
329 with the Odyssey® CLx Imager (LI-COR Biosciences). Mitochondrial enrichment and Western blotting
330 protocols were described previously [43].

331

332 **Immunofluorescence**

333 POE SH-SY5Y cells were reverse transfected with 50 nM siRNA in 96-well CellCarrier Ultra plates
334 according to the manufacturer's instructions and incubated for 72 h. Cells were then treated, fixed
335 and stained as per the screening protocol detailed above (for treatment concentrations and times,
336 see figures). Image intensities were not modified or pre-processed. Images are presented as

337 maximum projections of the pUb(Ser65) or PMPCB-488 channel for one field of view. Insets show
338 the Hoechst 33342 channel for the same field.
339
340 ***Drosophila* stocks and husbandry**
341 Flies were raised under standard conditions in a humidified, temperature-controlled incubator with
342 a 12h:12h light:dark cycle at 25°C, on food consisting of agar, cornmeal, molasses, propionic acid and
343 yeast. The following strains were obtained from the Bloomington *Drosophila* Stock Center
344 (RRID:SCR_006457): *mof* RNAi lines, P{TRiP.JF01701} (RRID:BDSC_31401); and P{TRiP.HMS00537}
345 (RRID:BDSC_58281); *nsl1* RNAi lines, P{TRiP.HMJ22458} (RRID:BDSC_58328); the pan-neuronal *nSyb-*
346 *GAL4* driver (RRID:BDSC_51941); and dopaminergic neuron driver (TH-GAL4; RRID:BDSC_8848); and
347 control (*lacZ*) RNAi P{GD936}v51446) from the Vienna *Drosophila* Resource Center
348 (RRID:SCR_013805). All experiments were conducted using male flies.
349
350 **Locomotor and lifespan assays**
351 The startle induced negative geotaxis (climbing) assay was performed using a counter-current
352 apparatus. Briefly, 20-23 males were placed into the first chamber, tapped to the bottom, and given
353 10 s to climb a 10 cm distance. This procedure was repeated five times (five chambers), and the
354 number of flies that has remained into each chamber counted. The weighted performance of several
355 group of flies for each genotype was normalized to the maximum possible score and expressed as
356 *Climbing index* [44].
357 For lifespan experiments, flies were grown under identical conditions at low-density. Progeny were
358 collected under very light anaesthesia and kept in tubes of approximately 20 males each, around 50-
359 100 in total. Flies were transferred every 2-3 days to fresh medium and the number of dead flies
360 recorded. Percent survival was calculated at the end of the experiment after correcting for any
361 accidental loss.
362
363 **Immunohistochemistry and sample preparation**
364 *Drosophila* brains were dissected from aged flies and immunostained as described previously [45].
365 Adult brains were dissected in PBS and fixed in 4% formaldehyde for 30 min on ice, permeabilized in
366 0.3% Triton X-100 for 3 times 20 min, and blocked with 0.3% Triton X-100 plus 4% goat serum in PBS
367 for 4 h at RT. Tissues were incubated with anti-tyrosine hydroxylase (Immunostar Inc. #22491),
368 diluted in 0.3% Triton X-100 plus 4% goat serum in PBS for 72 h at 4°C, then rinsed 3 times 20 min
369 with 0.3% Triton X-100 in PBS, and incubated with the appropriate fluorescent secondary antibodies
370 overnight at 4°C. The tissues were washed 2 times in PBS and mounted on slides using Prolong

371 Diamond Antifade mounting medium (Thermo Fisher Scientific). Brains were imaged with a Zeiss
372 LMS 880 confocal. Tyrosine hydroxylase-positive neurons were counted under blinded conditions.
373
374 **Statistical Analysis**
375 Intensity measurements from imaging experiments were normalised to SCR O/A for each
376 experiment and presented as a percentage. N numbers are shown in figure legends and refer to the
377 number of independent, replicate experiments. Within each experiment, the mean values of every
378 condition were calculated from a minimum of 3 technical replicates. Intensity measurements from
379 Western blot experiments were normalised to PINK1 O/A. GraphPad Prism 6 (La Jolla, California,
380 USA) was used for statistical analyses and graph production. Data were subjected to either one-way
381 or two-way ANOVA with Dunnett's post-hoc analysis for multiple comparisons, unless otherwise
382 stated. All error bars indicate mean ± standard deviation (SD) from replicate experiments.
383
384

Acknowledgements.

This work was supported in part by the UK Medical Research Council (MRC) funding to the Dementia Platform UK (MR/M02492X/1), MRC core funding to the High-Content Biology Platform at the MRC-UCL LMCB university unit (MC_U12266B) and MRC MBU (MC_UU_00015/6), and by UCL Translational Research Office administered seed funds. MS, EA, CM and DT are funded by MRC MR/N026004/1. DM is supported by an MRC CASE studentship (MR/P016677/1). AM, MB and PW are funded by ARUK (ARUK-2018DDI-UCL). MR was supported by the UK MRC through the award of Tenure-track Clinician Scientist Fellowship (MR/N008324/1). This work was supported in part by the Intramural Research Programs of the National Institute on Aging (NIA). We also acknowledge the support of the NIHR BRC award to University College London Hospitals, UCL. Finally, the authors would like to thank the Genome Aggregation Database (gnomAD) and the groups that provided exome and genome variant data to these resources. A full list of contributing groups can be found at https://gnomad.broadinstitute.org/about.

Author Contributions.

HPF, PL, JH, AW and PW conceived the idea. MS, DM, EA, AM, DT, MB, PW, JH, AW, MR, PL and HPF designed the experiments. MS, DM, EA, AM, NW, NW, KDS, SG, DZ, AP, DT, KP, CM, CB and HPF carried out analysis and experiments. MS, DM, EA, AM, PW, CM, AW, MR, PL and HPF wrote the manuscript, with input from all co-authors. HPF, PL and MR supervised the project.

Competing Interests: The authors declare that they have no conflict of interest

Correspondence and requests for materials should be addressed to h.plun-favreau@ucl.ac.uk.

410 **REFERENCES**

411 1. Hardy, J., Lewis, P., Revesz, T., Lees, A. & Paisan-Ruiz, C. The genetics of Parkinson's
412 syndromes: a critical review. *Curr. Opin. Genet. Dev.* **19**, 254–265 (2009).
413 2. Connolly, B. S. & Lang, A. E. Pharmacological treatment of Parkinson disease: A review. *JAMA*
414 *- J. Am. Med. Assoc.* **311**, 1670–1683 (2014).
415 3. Chang, D. *et al.* A meta-analysis of genome-wide association studies identifies 17 new
416 Parkinson's disease risk loci. *Nat. Genet.* (2017). doi:10.1038/ng.3955
417 4. Nalls, M. A. *et al.* Identification of novel risk loci, causal insights, and heritable risk for
418 Parkinson's disease: a meta-analysis of genome-wide association studies. *Lancet Neurol.* **18**,
419 1091–1102 (2019).
420 5. International Parkinson Disease Genomics Consortium, D. *et al.* Imputation of sequence
421 variants for identification of genetic risks for Parkinson's disease: a meta-analysis of genome-
422 wide association studies. *Lancet* (2011). doi:10.1016/S0140-6736(10)62345-8
423 6. Narendra, D., Tanaka, A., Suen, D.-F. & Youle, R. J. Parkin is recruited selectively to impaired
424 mitochondria and promotes their autophagy. *J. Cell Biol.* **183**, 795–803 (2008).
425 7. McWilliams, T. G. & Muqit, M. M. PINK1 and Parkin: emerging themes in mitochondrial
426 homeostasis. *Curr. Opin. Cell Biol.* **45**, 83–91 (2017).
427 8. Narendra, D. P. *et al.* PINK1 is selectively stabilized on impaired mitochondria to activate
428 Parkin. *PLoS Biol.* **8**, e1000298 (2010).
429 9. Kazlauskaite, A. *et al.* Parkin is activated by PINK1-dependent phosphorylation of ubiquitin at
430 Ser65. *Biochem. J.* **460**, 127–39 (2014).
431 10. Shiba-Fukushima, K. *et al.* Phosphorylation of Mitochondrial Polyubiquitin by PINK1 Promotes
432 Parkin Mitochondrial Tethering. *PLoS Genet.* **10**, e1004861 (2014).
433 11. Lazarou, M. *et al.* The ubiquitin kinase PINK1 recruits autophagy receptors to induce
434 mitophagy. *Nature* (2015). doi:10.1038/nature14893
435 12. Plotegher, N. & Duchen, M. R. Crosstalk between Lysosomes and Mitochondria in Parkinson's
436 Disease. *Front. Cell Dev. Biol.* (2017). doi:10.3389/fcell.2017.00110
437 13. Chatterjee, A. *et al.* MOF Acetyl Transferase Regulates Transcription and Respiration in
438 Mitochondria. *Cell* **167**, 722-738.e23 (2016).
439 14. Giambartolomei, C. *et al.* Bayesian Test for Colocalisation between Pairs of Genetic
440 Association Studies Using Summary Statistics. *PLoS Genet.* (2014).
441 doi:10.1371/journal.pgen.1004383
442 15. Ramasamy, A. *et al.* Genetic variability in the regulation of gene expression in ten regions of
443 the human brain. *Nat. Neurosci.* (2014). doi:10.1038/nn.3801

444 16. Lonsdale, J., Thomas, J., Salvatore, M., Phillips, R. & Lo, E. The Genotype-Tissue Expression
445 (GTEx) project : Nature Genetics : Nature Publishing Group. *Nature* (2013).
446 17. Kia, D. A. *et al.* Integration of eQTL and Parkinson ' s disease GWAS data implicates 11 disease
447 genes. (2019).
448 18. Ferrari, R. *et al.* Stratification of candidate genes for Parkinson's disease using weighted
449 protein-protein interaction network analysis. *BMC Genomics* (2018). doi:10.1186/s12864-
450 018-4804-9
451 19. Nalls, M. A. *et al.* Large-scale meta-analysis of genome-wide association data identifies six
452 new risk loci for Parkinson's disease. *Nat. Genet.* (2014). doi:10.1038/ng.3043
453 20. Robak, L. A. *et al.* Excessive burden of lysosomal storage disorder gene variants in Parkinson's
454 disease. *Brain* (2017). doi:10.1093/brain/awx285
455 21. Hou, X. *et al.* Age- and disease-dependent increase of the mitophagy marker phospho-
456 ubiquitin in normal aging and Lewy body disease. *Autophagy* (2018).
457 doi:10.1080/15548627.2018.1461294
458 22. Gusev, A. *et al.* Integrative approaches for large-scale transcriptome-wide association studies.
459 *Nat. Genet.* (2016). doi:10.1038/ng.3506
460 23. Simon, R. P., Robaa, D., Alhalabi, Z., Sippl, W. & Jung, M. KATching-Up on Small Molecule
461 Modulators of Lysine Acetyltransferases. *J. Med. Chem.* **59**, 1249–1270 (2016).
462 24. Sheikh, B. N. & Akhtar, A. The many lives of KATs — detectors, integrators and modulators of
463 the cellular environment. *Nat. Rev. Genet.* **20**, 7–23 (2019).
464 25. Bertolin, G. *et al.* The TOMM machinery is a molecular switch in PINK1 and PARK2/PARKIN-
465 dependent mitochondrial clearance. *Autophagy* **9**, 1801–1817 (2013).
466 26. Raja, S. J. *et al.* The nonspecific lethal complex is a transcriptional regulator in Drosophila.
467 *Mol. Cell* **38**, 827–841 (2010).
468 27. Wray, S. & Lewis, P. A. A tangled web - tau and sporadic Parkinson's disease. *Frontiers in*
469 *Psychiatry* (2010). doi:10.3389/fpsyt.2010.00150
470 28. Stefansson, H. *et al.* A common inversion under selection in Europeans. *Nat. Genet.* (2005).
471 doi:10.1038/ng1508
472 29. Zody, M. C. *et al.* Evolutionary toggling of the MAPT 17q21.31 inversion region. *Nat. Genet.*
473 (2008). doi:10.1038/ng.193
474 30. Pittman, A. M. *et al.* Linkage disequilibrium fine mapping and haplotype association analysis
475 of the tau gene in progressive supranuclear palsy and corticobasal degeneration. *J. Med.*
476 *Genet.* (2005). doi:10.1136/jmg.2005.031377
477 31. Hutton, M. *et al.* Association of missense and 5'-splice-site mutations in tau with the

478 inherited dementia FTDP-17. *Nature* (1998). doi:10.1038/31508
479 32. Guelfi, S. *et al.* Regulatory sites for known and novel splicing in human basal ganglia are
480 enriched for disease-relevant information. *bioRxiv* (2019). doi:10.1101/591156
481 33. Fung, H. C. *et al.* Genome-wide genotyping in Parkinson's disease and neurologically normal
482 controls: first stage analysis and public release of data. *Lancet Neurol.* (2006).
483 doi:10.1016/S1474-4422(06)70578-6
484 34. Dong, X. *et al.* Enhancers active in dopamine neurons are a primary link between genetic
485 variation and neuropsychiatric disease. *Nat. Neurosci.* (2018). doi:10.1038/s41593-018-0223-
486 0
487 35. Lai, Y. *et al.* Phosphoproteomic screening identifies Rab GTP ases as novel downstream
488 targets of PINK 1 . *EMBO J.* (2015). doi:10.15252/embj.201591593
489 36. Sheikh, B. N., Guhathakurta, S. & Akhtar, A. The non-specific lethal (NSL) complex at the
490 crossroads of transcriptional control and cellular homeostasis . *EMBO Rep.* (2019).
491 doi:10.15252/embr.201847630
492 37. Swatek, K. N. & Komander, D. Ubiquitin modifications. *Cell Res.* (2016).
493 doi:10.1038/cr.2016.39
494 38. Valente, E. M. *et al.* Hereditary early-onset Parkinson's disease caused by mutations in
495 PINK1. *Sci. (New York, NY)* **304**, 1158–1160 (2004).
496 39. Kitada, T. *et al.* Mutations in the parkin gene cause autosomal recessive juvenile
497 parkinsonism. *Nature* (1998). doi:10.1038/33416
498 40. Chu, C. T. Mechanisms of selective autophagy and mitophagy: Implications for
499 neurodegenerative diseases. *Neurobiology of Disease* (2019). doi:10.1016/j.nbd.2018.07.015
500 41. Pruim, R. J. *et al.* LocusZoom: Regional visualization of genome-wide association scan results.
501 in *Bioinformatics* (2011). doi:10.1093/bioinformatics/btq419
502 42. Ardley, H. C. *et al.* Inhibition of proteasomal activity causes inclusion formation in neuronal
503 and non-neuronal cells overexpressing Parkin. *Mol. Biol. Cell* **14**, 4541–4556 (2003).
504 43. Soutar, M. P. M. *et al.* AKT signalling selectively regulates PINK1 mitophagy in SHSY5Y cells
505 and human iPSC-derived neurons. 1–11 (2018). doi:10.1038/s41598-018-26949-6
506 44. Greene, J. C. *et al.* Mitochondrial pathology and apoptotic muscle degeneration in Drosophila
507 parkin mutants. *Proc. Natl. Acad. Sci. U. S. A.* **100**, 4078–4083 (2003).
508 45. Whitworth, A. J. *et al.* Increased glutathione S-transferase activity rescues dopaminergic
509 neuron loss in a Drosophila model of Parkinson's disease. *Proc. Natl. Acad. Sci. U. S. A.* **102**,
510 8024–8029 (2005).
511 46. Lek, M. *et al.* Analysis of protein-coding genetic variation in 60,706 humans. *Nature* (2016).

512 doi:10.1038/nature19057

513

514 **FIGURE LEGENDS**

515

516 **Figure 1 - Selection of the genes for the PINK1-dependent mitophagy screening.**

517 **A.** The heat-map represents increasing evidence for gene prioritization (white, light blue, and dark
518 blue: one, two, and three evidences, respectively). ColB = coloc analysis using Braineac, ColG = coloc
519 analysis using GTEx, WPPINA = weighted protein interaction network; GWAS = genes prioritised in
520 PD-GWAS [3].

521 **B.** Genes prioritised by means of multiple prediction techniques, grouped based on the types of
522 evidences.

523 **C.** Venn diagram highlighting the three genes prioritised by means of three prediction techniques.

524

525 **Figure 2 – High content mitophagy screen identifies KAT8 as a modulator of pUb(Ser65) levels.**

526 **A.** pUb(Ser65) Z-scores of one representative mitophagy screen plate.

527 **B.** Overview of the PD GWAS genetic signal at the *KAT8* locus.

528

529 **Figure 3 - KAT8 knockdown decreases pUb(Ser65).**

530 **A.** Representative images of pUb(Ser65) following treatment of SCR, PINK1 and KAT8 siRNA KD POE
531 SH-SY5Y with 1 µM O/A for 3 h. Insets show the nuclei for the same fields. Scale bar: 20 µm.

532 **B.** Quantification of pUb(Ser65) levels in A (n=3, two-way ANOVA with Dunnett's correction).

533 **C.** Representative IB of mitochondrial fractions from SCR, PINK1 and KAT8 KD POE SH-SY5Y treated
534 with 1 µM O/A for 1.5 or 3 h.

535 **D.** Quantification of pUb(Ser65) in C (n=5, one-way ANOVA with Dunnett's correction).

536 **E.** pUb(Ser65) Z-scores of one representative KAT screen plate. See Supplementary Table 4 for the
537 complete list of the genes screened.

538 Data are shown as mean ± SD.

539

540 **Figure 4 – Knockdown of the mitochondrial components of the NSL complex reduces pUb(Ser65)**
541 **levels.**

542 **A.** Schematic representation of the NSL complex.

543 **B, C.** Quantification of pUb(Ser65) following treatment of SCR, PINK1 or NSL components siRNA KD
544 POE SH-SY5Y cells with 1 µM O/A for 1.5 h (B) or 3 h (C). Data are shown as mean ± SD; n=6, one-way
545 ANOVA with Dunnett's correction.

546

547 **Figure 5 - KANSL1 knockdown decreases pUb(Ser65).**

548 **A.** Representative images of pUb(Ser65) following treatment of SCR, PINK1 and KANSL1 KD POE SH-
549 SY5Y cells with 1 µM O/A for 3 h. Insets show the nuclei for the same fields. Scale bar: 20 µm.

550 **B.** Quantification of pUb(Ser65) in A (n=3, two-way ANOVA with Dunnett's correction).

551 **C**. Representative IB of mitochondrial fractions from SCR, PINK1 and KANSL1 KD POE SH-SY5Y
552 treated with 1 µM O/A for 1.5 or 3 h.

553 **D.** Quantification of pUb(Ser65) in C (n=5, one-way ANOVA with Dunnett's correction).

554 Data are shown as mean ± SD.

555

556 **Figure 6 - KANSL1 and KAT8 knockdown decrease pUb(Ser65).**

557 **A.** Representative images of pUb(Ser65) (green) following treatment of SCR, PINK1, KAT8 and
558 KANSL1 KD POE SH-SY5Y cells with 1 µM O/A for 0-7 h. Insets show the nuclei for the same fields.
559 Scale bar: 20 µm.

560 **B.** Quantification of pUb(Ser65) in A (n=6, two-way ANOVA with Dunnett's correction).

561 Data are shown as mean ± SD.

562

563 **Figure 7 - KANSL1 and KAT8 knockdown decrease mitochondrial clearance.**

564 **A.** Representative images of PMPCB (green) and nuclei (blue) following treatment of SCR, PINK1,
565 KAT8 and KANSL1 KD POE SH-SY5Y cells with 1 µM O/A for 0, 3, 6, 9 h. Scale bar: 10 µm.

566 **B.** Quantification of the number of PMPCB spots in A (n=5, two-way ANOVA with Dunnett's
567 correction).

568 Data are shown as mean ± SD.

569

570 **Figure 8 - ASE sites in KANSL1 in LD with the H1/H2 SNP.**

571 **A.** ASEs derived from putamen and substantia nigra in high linkage disequilibrium with the H1/H2
572 tagging SNP, rs12185268 and their position along the *KANSL1* gene. The missense variants track
573 displays the variants annotated as missense by gnomAD v2.1.1 [46]. The valid track displays the
574 heterozygous sites (orange = missense) with an average read depth greater than 15 reads across all
575 samples, which were examined for ASE. The topmost track displays the FDR-corrected minimum -
576 log10 p-value across samples for the sites that show an ASE in at least one sample.

577 B. Conservation of the KANSL1 protein across species. The four coding variants in the *KANSL1* gene
578 are in high LD (r2 >0.8) with the H1/H2 haplotypes.

579

580 **Figure 9. High content mitophagy screening of the ORFs on the 17q21 locus identifies only KANSL1**
581 **as a modulator of pUb(Ser65) levels.**
582 pUb(Ser65) Z-scores of one representative 17q21 locus screen plate. See Supplementary Table 8 for
583 the complete list of the genes screened.
584
585 **EXTENDED FIGURE LEGENDS**
586 **Extended Data Figure 1. High Content siRNA Screen for modulators of pUb(Ser65).**
587 **A.** Workflow of the high content screen for O/A-induced pUb(Ser65) levels.
588 **B.** Fold decrease in TOM20 levels following 1.5 and 3 h treatment with 0.1, 1 and 10 µM O/A,
589 compared to DMSO control.
590 **C.** Representative images of TOM20 and pUb(Ser65) following 3 h treatment of SCR KD POE SH-SY5Y
591 cells with 10 µM O/A. Scale bar: 20 µm.
592 **D.** Quantification of the co-localization in **C** as % of TOM20-positive pUb(Ser65) spots. Graph shows
593 all replicates of non-transfected, SCR, PINK1 and PLK1 KD for 3 independent experiments.
594 **E.** Representative images of pUb(Ser65) following treatment of SCR and PINK1 KD POE SH-SY5Y cells
595 with 10 µM O/A for 3 h. Scale bar: 20 µm.
596 **F.** Quantification of pUb(Ser65) in **E** (n=6, two-way ANOVA with Tukey's multiple comparisons test).
597 **G.** Representative analysis of integrated intensity of pUb(Ser65)and TOM20 for a single HCS plate.
598 **H.** pUb(Ser65) Z-scores of the two other replicate screen plates.
599 Data are shown as mean ± SD.
600
601 **Extended Data Figure 2. Image processing workflow of the high content screen for O/A induced**
602 **pUb(Ser65).**
603 Images were loaded as maximum projections. The Hoechst 33342 channel was used to find the
604 nuclei and border nuclei were excluded. The cytoplasm was then found on the calculated Hoechst +
605 TOM20-568 image. The pUb(Ser65)-488 spots were identified within the whole cell and their
606 intensity measured. The outputs of the analysis were the number of nuclei selected and the mean
607 integrated pUb(Ser65) intensity, calculated as the area of the cell covered by pUb(Ser65) spots x
608 corrected intensity of the spots. Analysis parameters for each building block of the Columbus
609 workflow are detailed in the boxes.
610
611 **Extended Data Figure 3. KAT8 knockdown has no effect on cell viability.**
612 **A.** Representative images of nuclei following treatment of SCR, PINK1 and PLK1 siRNA KD POE SH-
613 SY5Y cells with 10 µM O/A for 3 h. Scale bar: 20 µm.

614 **B.** Quantification of the number of nuclei in A (n=6, two-way ANOVA with Tukey's multiple
615 comparisons test).
616 **C.** Z-scores of a representative screen plate showing that KAT8 or PINK1 siRNA KD don't affect cell
617 viability, on the contrary to PLK-1 KD.
618 Data are shown as mean ± SD.
619
620 **Extended Data Figure 4. KAT8 eQTLs colocalise with SNPs associated with PD risk**
621 The x-axis displays the physical position on chromosome 16 in megabases. The minus log p-values
622 are plotted for every SNP present in both the PD GWAS [3] and *KAT8* eQTLs derived from the GTEx V7
623 caudate data. The p-values for the PD GWAS are plotted in yellow and p-values for *KAT8* eQTLs are
624 plotted in blue.
625
626 **Extended Data Figure 5. KAT8 knockdown decreases pUb(Ser65) levels.**
627 **A.** Representative images of pUb(Ser65) following treatment of SCR, PINK1 and KAT8 siRNA KD POE
628 SH-SY5Y with 10 µM O/A for 3 h. Insets show nuclear staining for the same fields. Scale bar: 20 µm.
629 **B.** Quantification of pUb(Ser65) levels in A (n=3, two-way ANOVA with Dunnett's correction).
630 **C.** Representative IB of mitochondrial fractions from SCR, PINK1 and KAT8 KD POE SH-SY5Y treated
631 with 10 µM O/A for 1.5 or 3 h.
632 **D, E.** Quantification of pUb(Ser65) (**D**) and KAT8 levels (**E**) in C (n=5, one-way ANOVA with Dunnett's
633 correction).
634 Data are shown as mean ± SD.
635
636 **Extended Data Figure 6. Neuronal loss of *mof* or *nsl1* causes locomotor deficit, shortened lifespan**
637 **and neurodegeneration.**
638 **A, B.** Climbing ability of pan-neuronal (*nSyb-GAL4*) driven knockdown of *mof* (**A**) or *nsl1* (**B**)
639 measured at the indicated age of adults, compared to control RNAi (A: Kruskal-Wallis test, with
640 Dunn's post-hoc multiple comparisons; B: Mann-Whitney test).
641 **C, D.** Lifespan of ***mof* (C) or *nsl1* (D)** pan-neuronal knockdown (*nSyb-GAL4*) compared to control RNAi
642 (Log-rank (Mantel-Cox) test).
643 **E, F.** Quantification of dopaminergic neurons (PPL1 cluster) after pan-neuronal or dopaminergic (DA)
644 neuron (*TH-GAL4*) driven depletion of *mof* (**E**), nsl1 (**F**), or control RNAi. Representative images of
645 PPL1 neurons (as bounded by the box) under depletion conditions are shown. Flies were aged 30
646 days, except for pan-neuronal *nsl1* kd which are 16-days-old. Scale bar: 20 µm; Mann-Whitney test.
647 For all tests, n numbers are indicated in the graphs; p<0.0001 = ****; p<0.001 = ***.

648

649 **Extended Data Figure 7. Overview of the PD GWAS genetic signal at the *MAPT* locus.**

650 **A.** *MAPT* primary GWAS signal.

651 **B.** *MAPT* conditional GWAS signal.

652

653 **Extended Data Figure 8. ASE sites in *MAPT* in LD with the H1/H2 SNP.**

654 ASEs derived from putamen and substantia nigra that are in LD with the H1/H2 tagging SNP,
655 rs12185268 and their position along the *MAPT* gene. The missense variants track displays the
656 variants annotated as missense by gnomAD v2.1.1 [46]. The valid track displays the heterozygous sites
657 (orange = missense) with an average read depth greater than 15 reads across all samples, in LD with
658 H1/H2, which were examined for ASE. The topmost track displays the –log10 scale for the minimum
659 FDR across samples for the sites that show an ASE in at least one sample.

A

Gene	ColB/G	WPPINA	GWAS
CAB39L	X		
CCNT2			X
CD38	X		X
CTSB	X	X	X
DDRGK1			X
DGKQ			X
GALC	X		X
GBA		X	X
GPNMB	X		X
HSD3B7	X		
INPP5F		X	
KAT8	X	X	X
KLHL7	X		X
LRRK2		X	X
LSM7	X		X
MAPT		X	X
NCKIPSD	X	X	X
NSF		X	
NUCKS1	X		X
NUPL2	X		X
PDLIM2	X		X
PM20D1	X		
RAB7L1	X	X	
SH3GL2		X	X
SLC41A1	X		X
SNCA			X
SPPL2B	X		
STK39			X
VAMP4	X		
WDR6	X		
ZNF646			X

B

Prediction Technique	Genes
ColB/G; GWAS; WPPINA	*CTSB* *KAT8* *NCKIPSD*
ColB/G; GWAS	*CD38* *GALC* *GPNMB* *KLHL7* *LSM7* *NUCKS1* *NUPL2* *PDLIM2* *SLC41A1*
ColB/G; WPPINA	*RAB7L1*
GWAS; WPPINA	*GBA* *LRRK2* *MAPT* *SH3GL2*

C

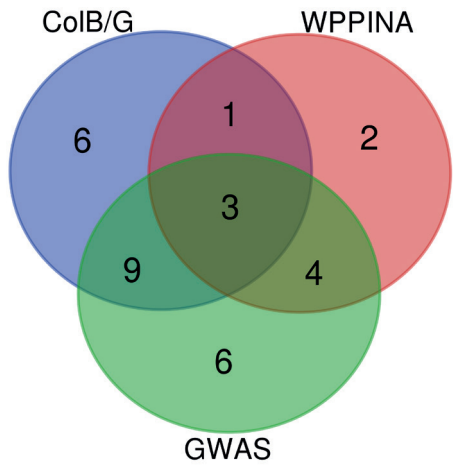

Figure 1 - Selection of the genes for the PINK1-dependent mitophagy screening.

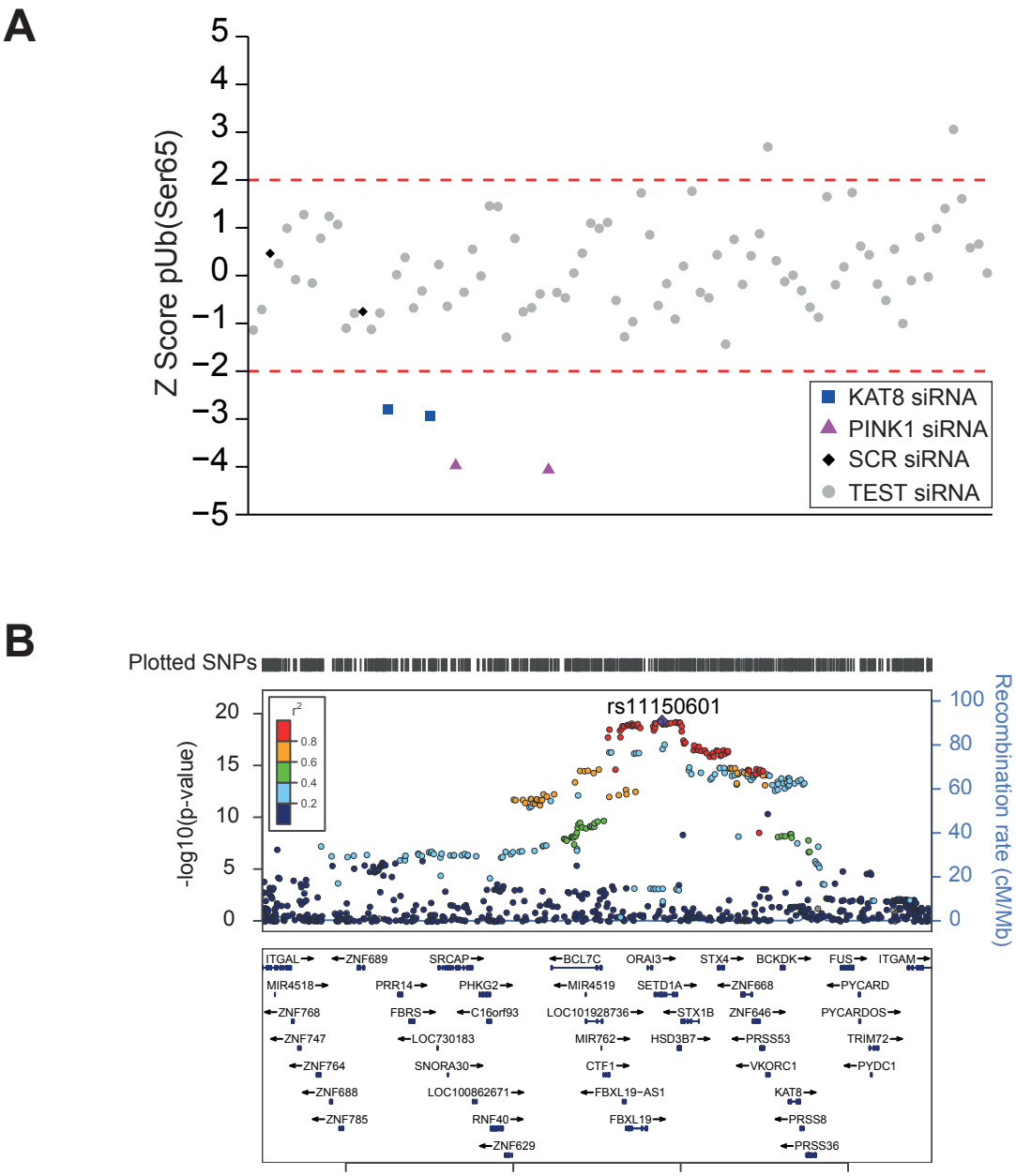

Figure 2 – High content mitophagy screen identifies KAT8 as a modulator of pUb(Ser65) levels.

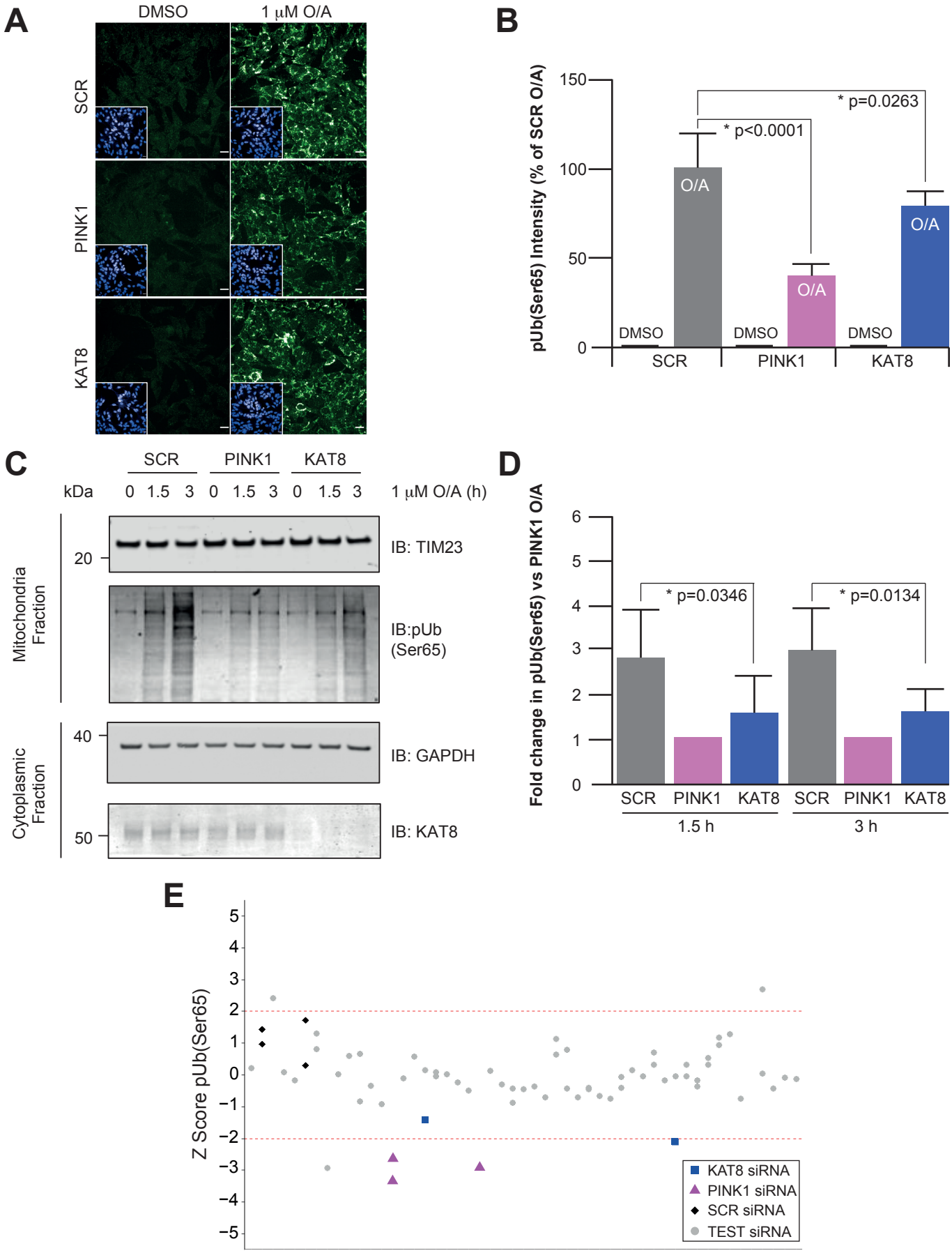

Figure 3 - KAT8 knockdown decreases pUb(Ser65).

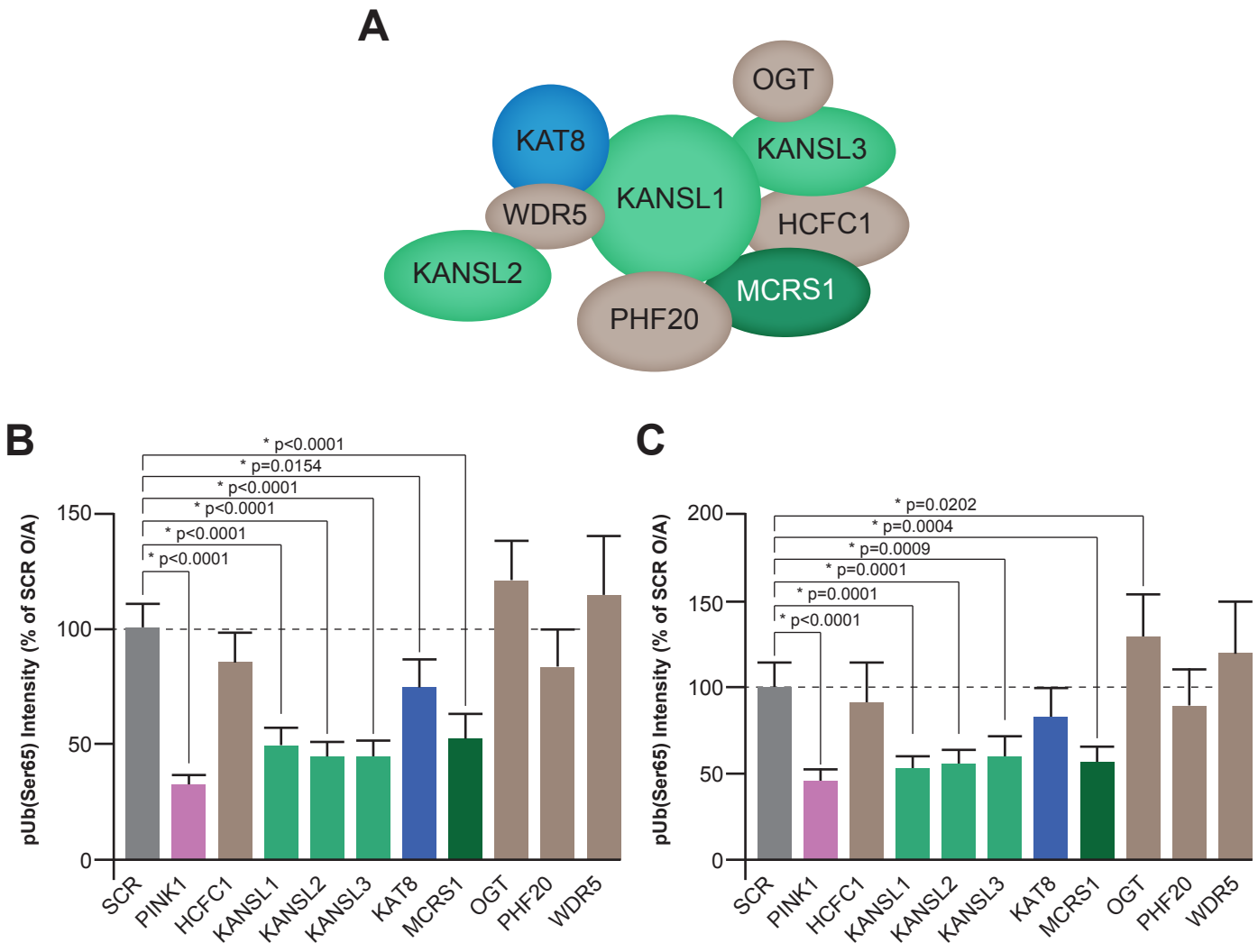

Figure 4 – Knockdown of the mitochondrial components of the NSL complex reduces pUb(Ser65) levels.

.

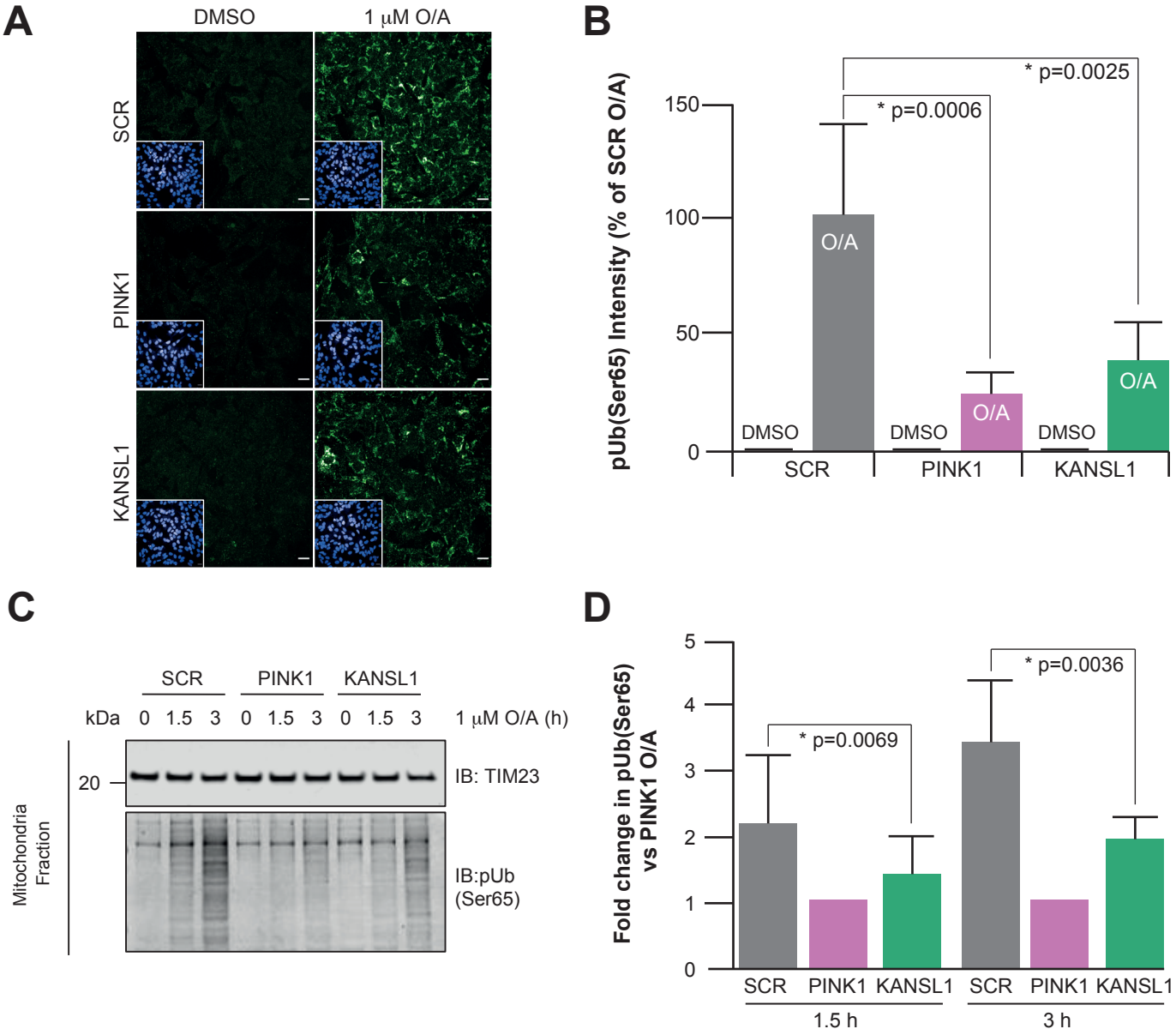

Figure 5 - KANSL1 knockdown decreases pUb(Ser65).

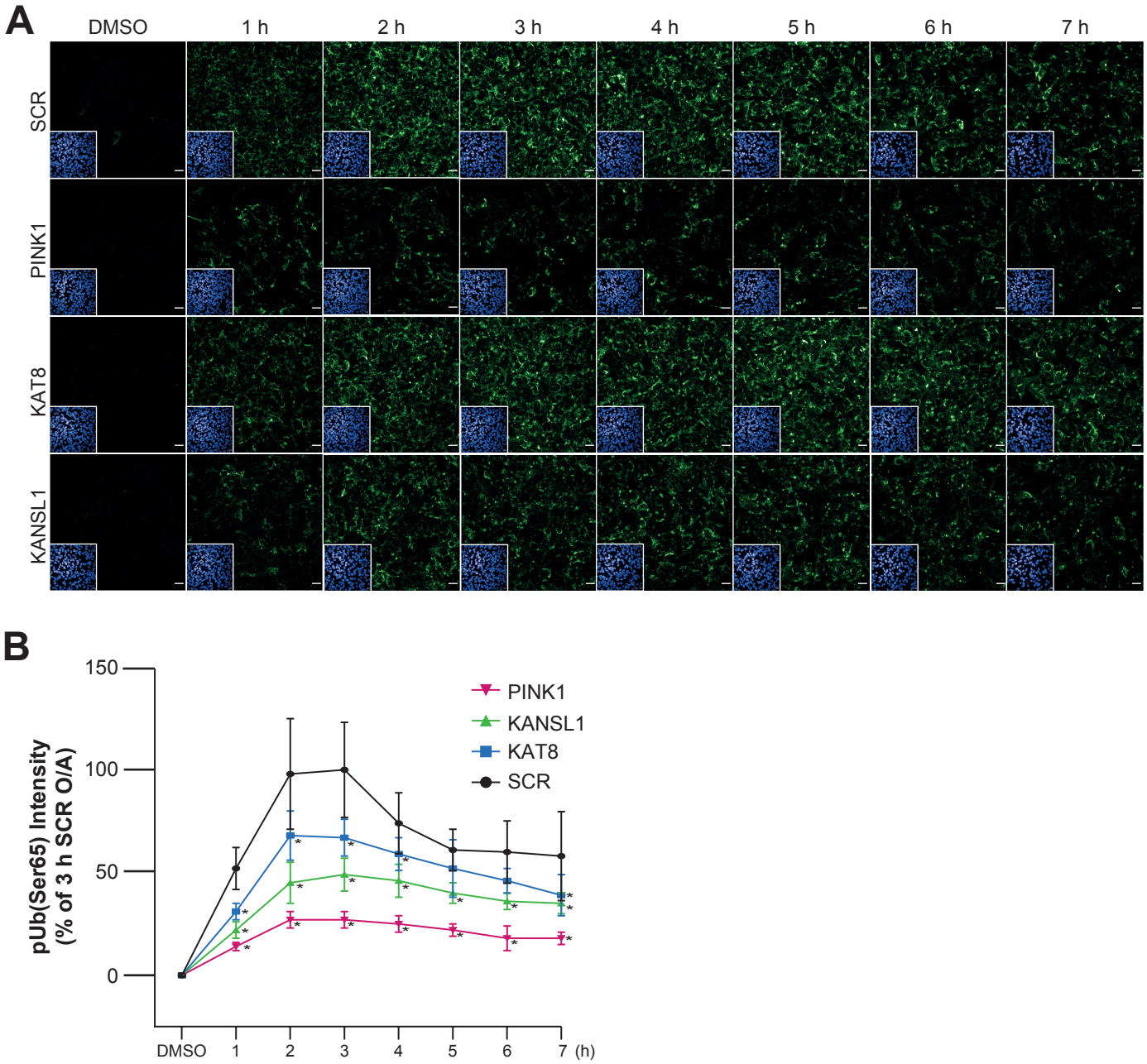

Figure 6 - KANSL1 and KAT8 knockdown decrease pUb(Ser65).

A

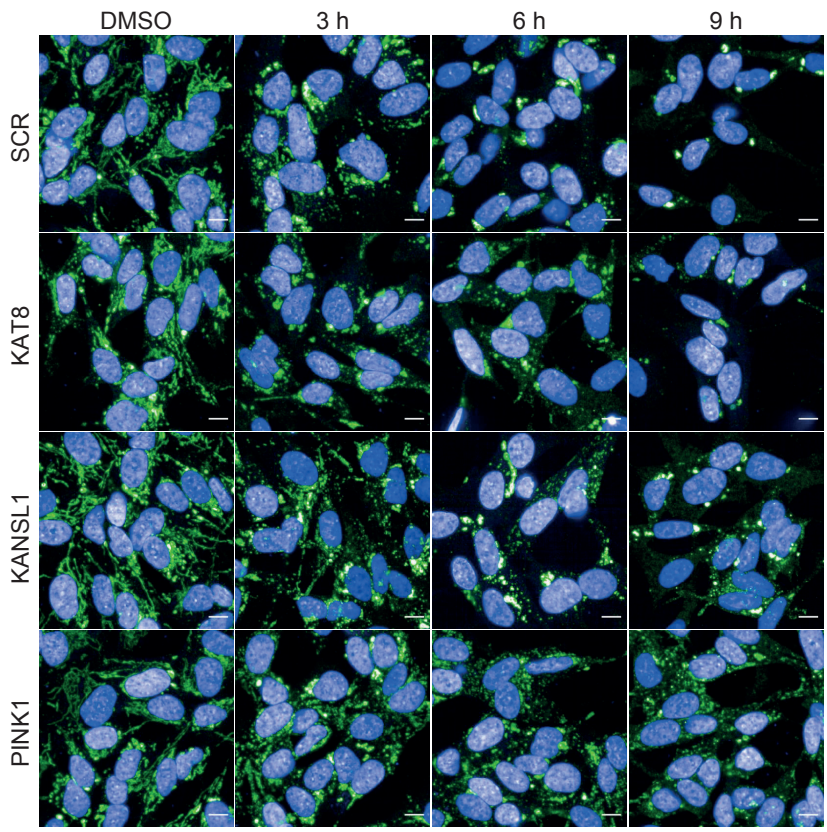

B

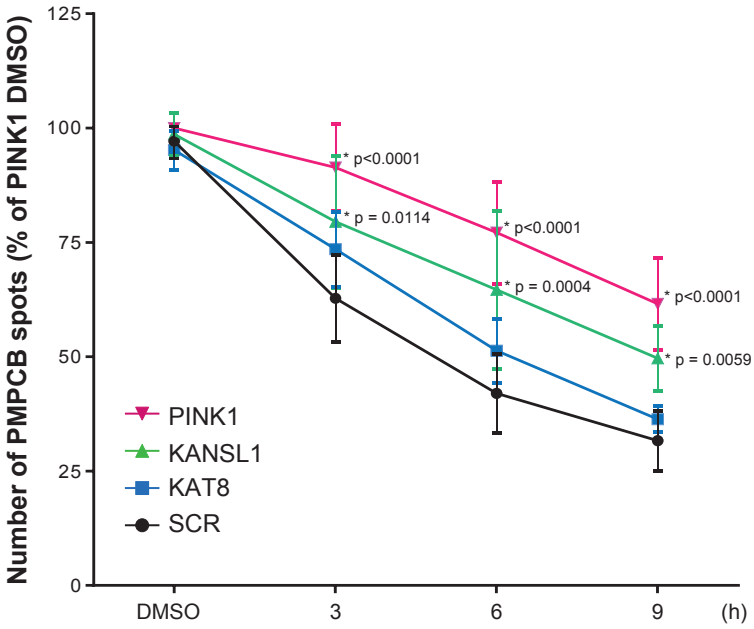

Figure 7 – KANSL1 and KAT8 knockdown decrease mitochondrial clearance.

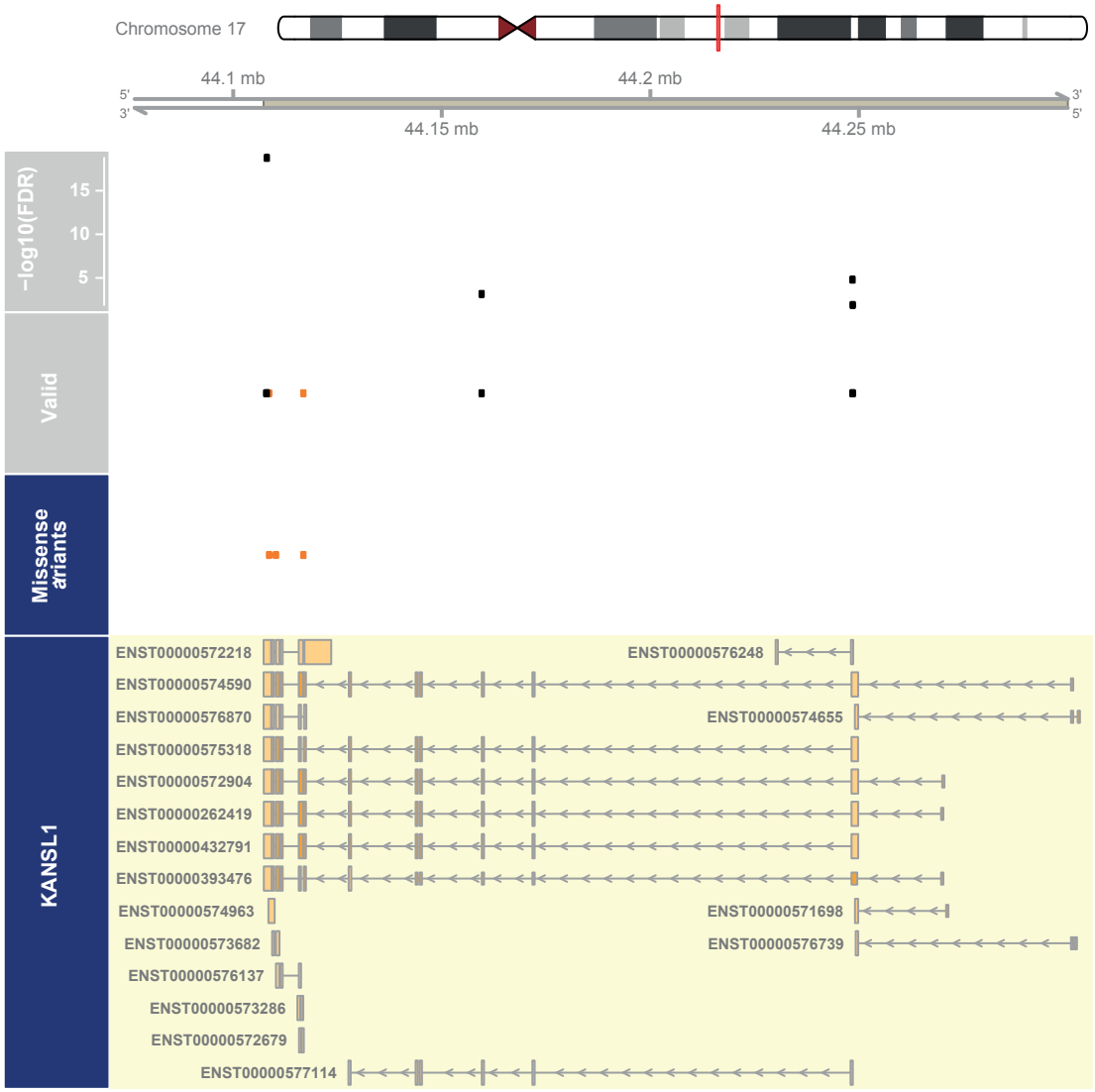

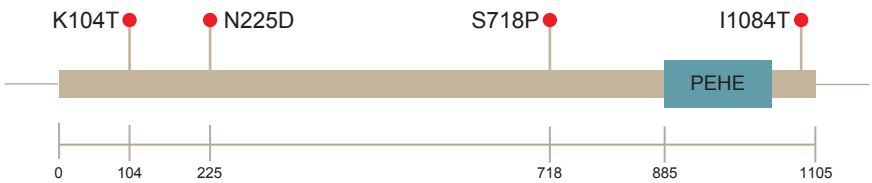

	Haplotype	K104T	N225D	S718P	I1084T	*% hap*	
Homo sapiens	H1	K	N	S	I	*0.79*	***PD associated***
	H2	T	D	P	T	*0.19*	
	H2	K	N	P	T	*0.015*	
Pan troglodytes	H2	K	N	P	T		
Pongo pygmaeus	H2	K	N	P	T		
Macaca mulatta	n/a	K	N	P	T		
Mus musculus	n/a	K	N	P	V		

Figure 8 - ASE sites in KANSL1 in LD with the H1/H2 SNP.

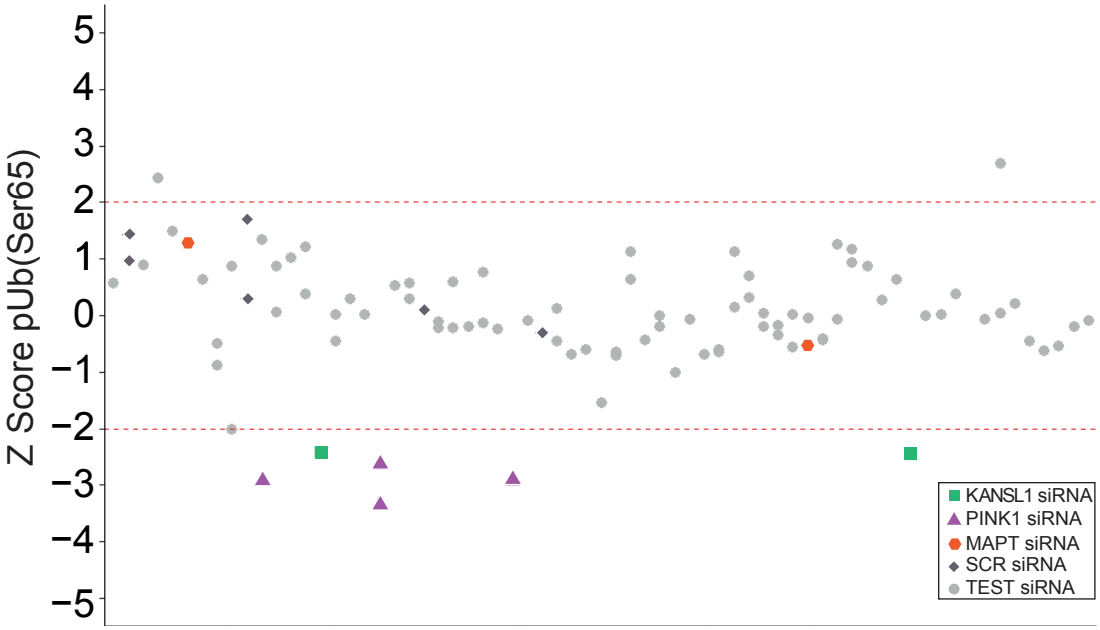

Figure 9 – High content mitophagy screening of the ORFs on the the 17q21 locus identifies only KANSL1 as a modulator of pUb(Ser65) levels.

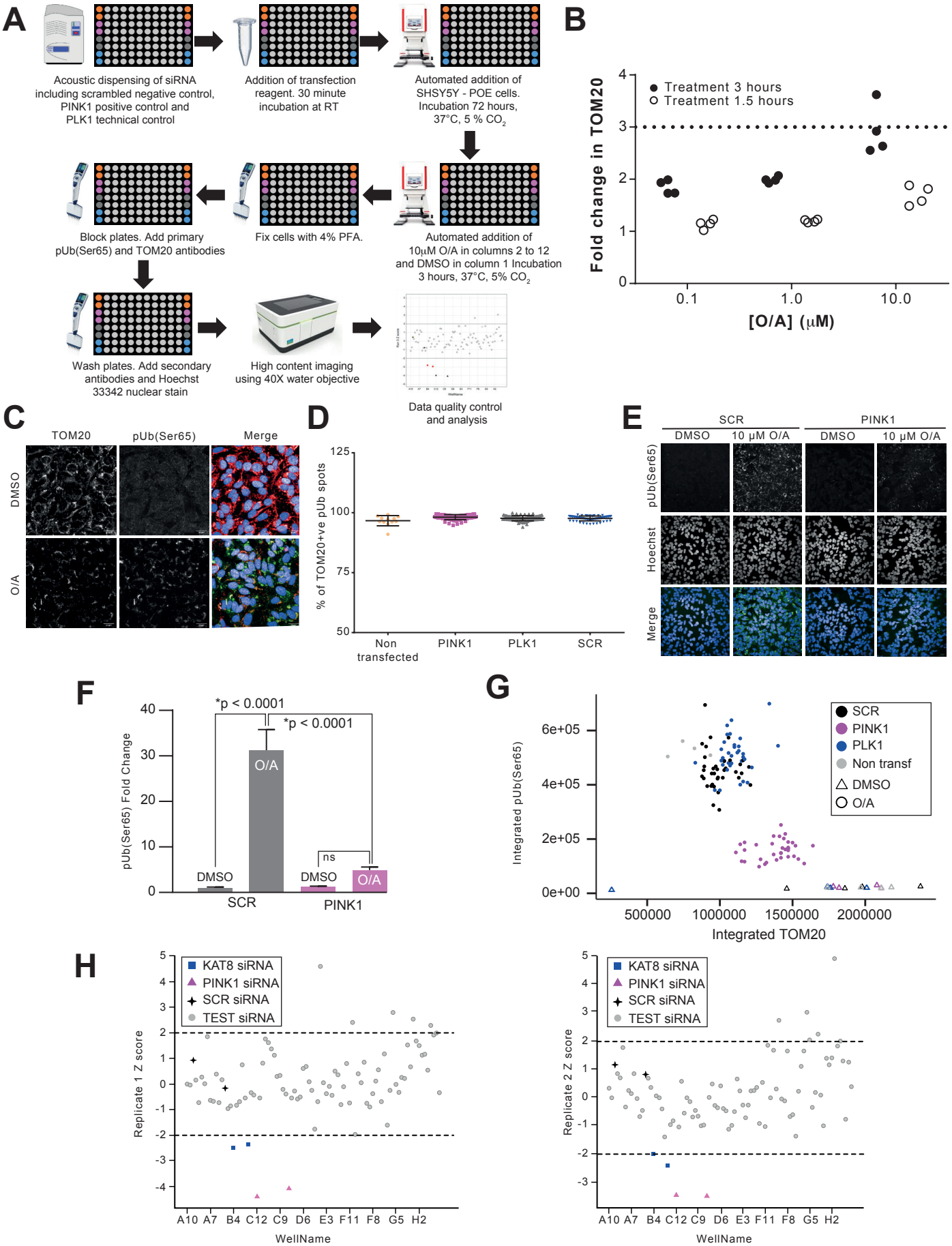

Extended Data Figure 1. High Content siRNA Screen for modulators of pUb(Ser65).

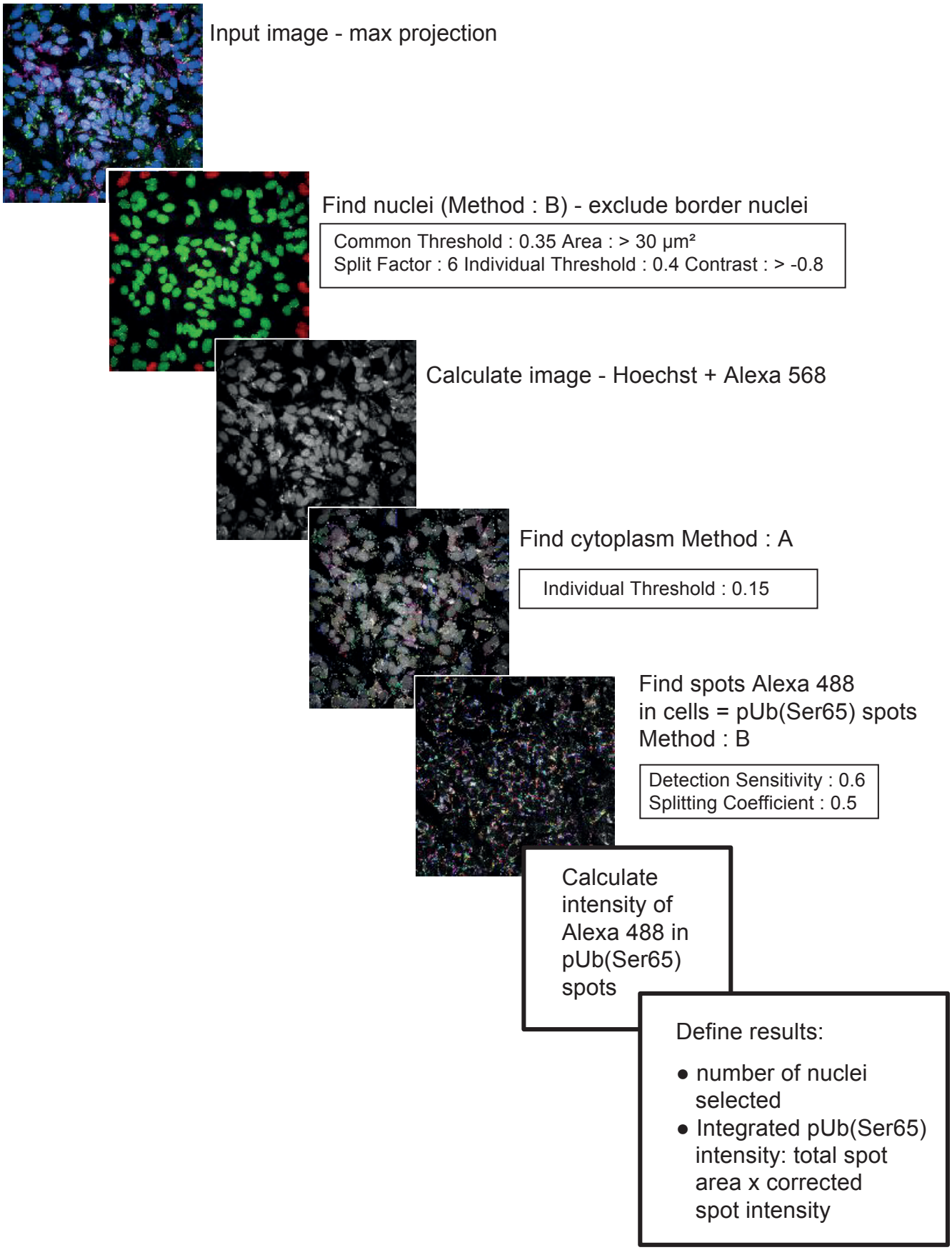

Extended Data Figure 2. Image processing workflow of the high content screen for O/A induced pUb(Ser65).

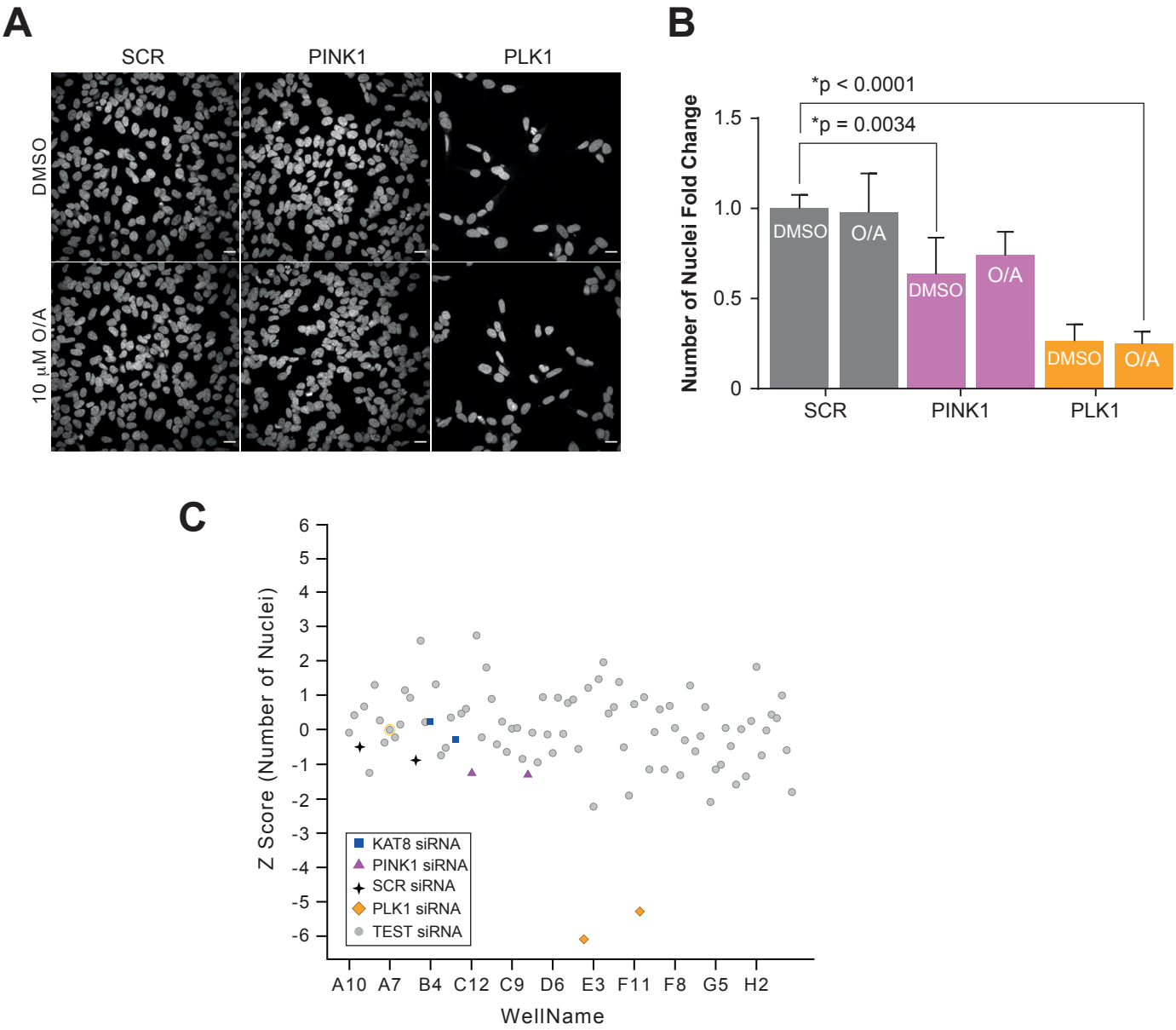

Extended Data Figure 3. KAT8 knockdown has no effect on cell viability.

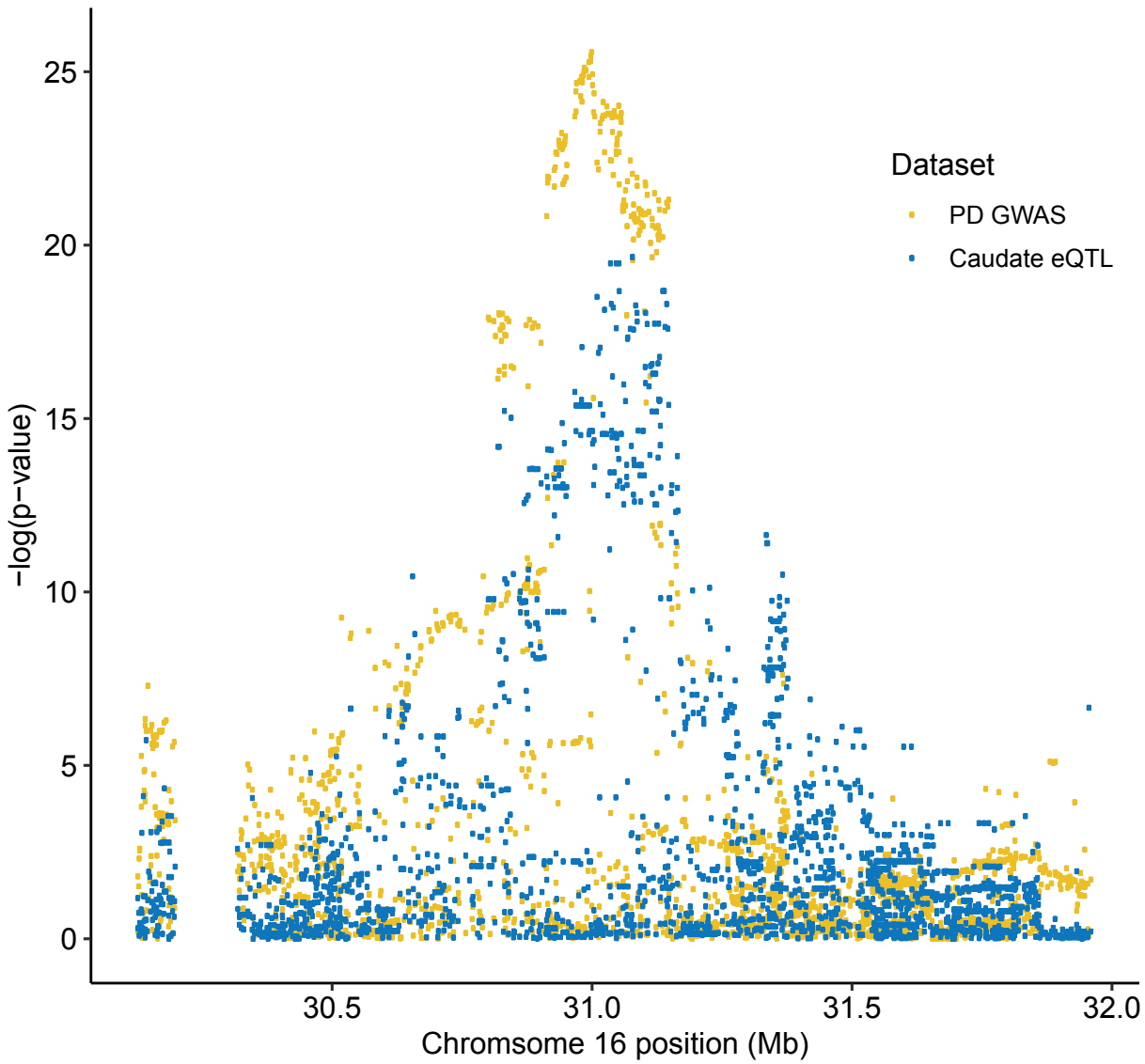

Extended Data Figure 4. KAT8 eQTLs colocalise with SNPs associated with PD risk.

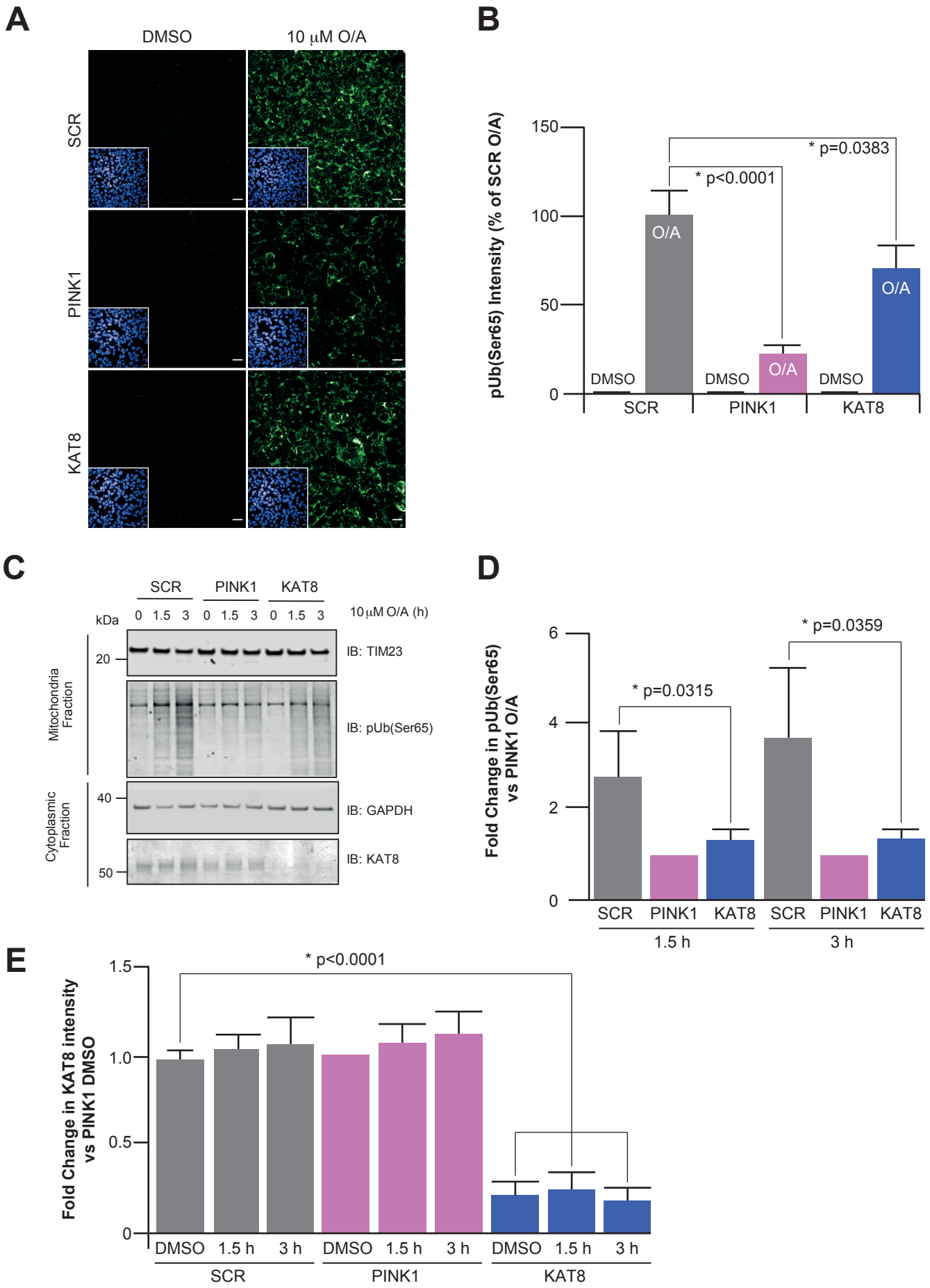

Extended Data Figure 5. KAT8 knockdown decreases pUb(Ser65) levels.

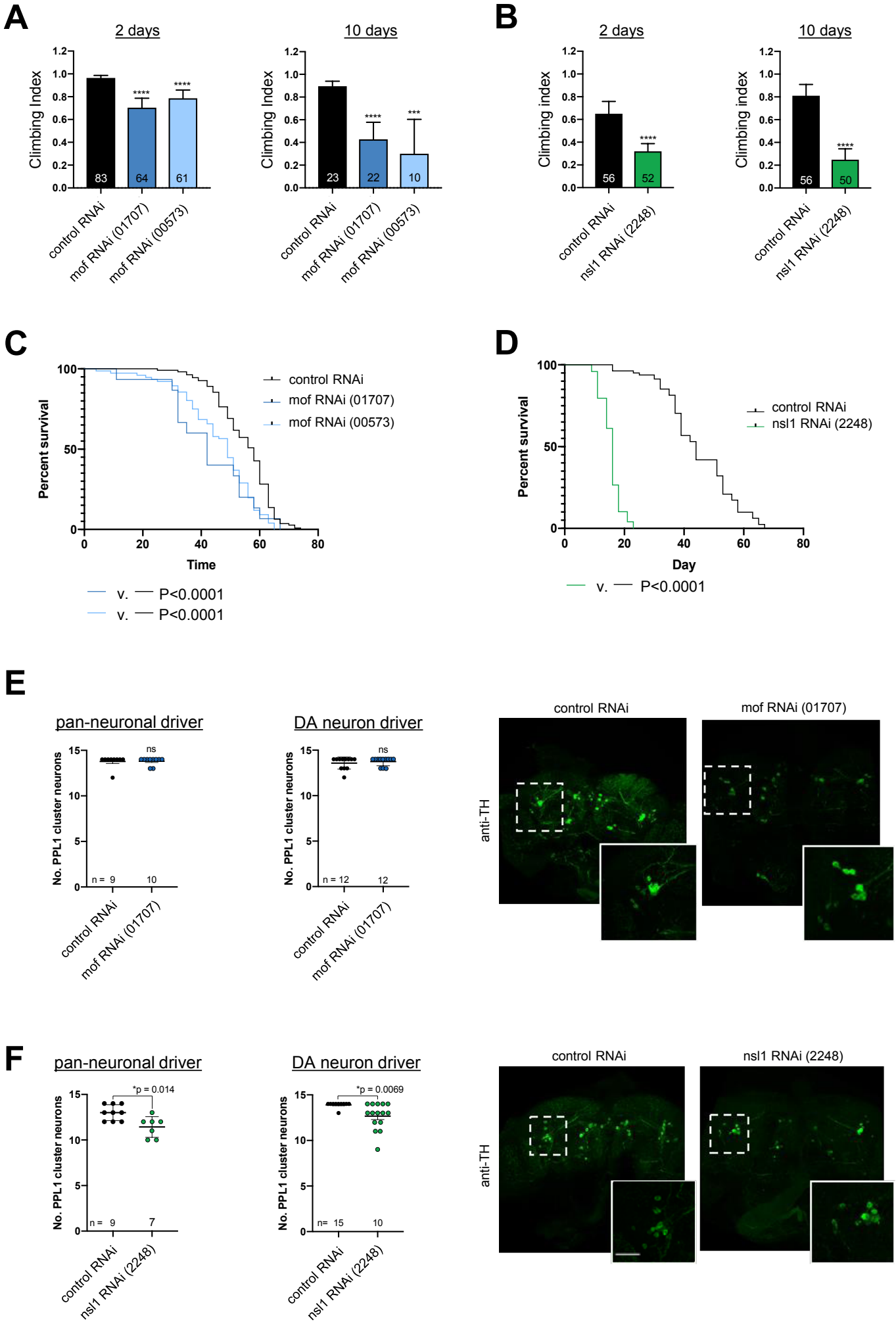

Extended Data Figure 6. Neuronal loss of *mof* or *nsl1* causes locomotor deficit, shortened lifespan and neurodegeneration.

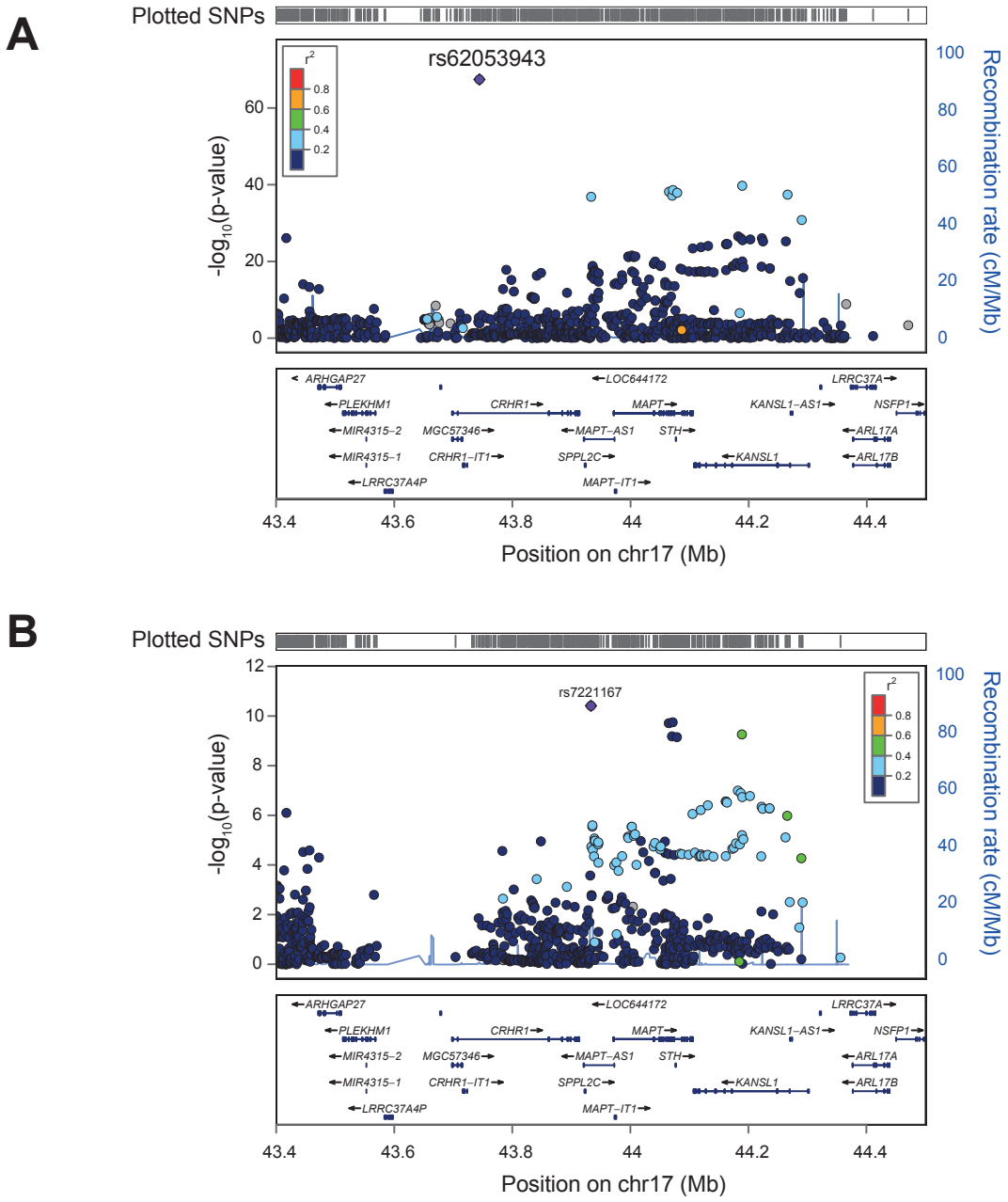

Extended Data Figure 7. Overview of the PD GWAS genetic signal at the *MAPT* locus.

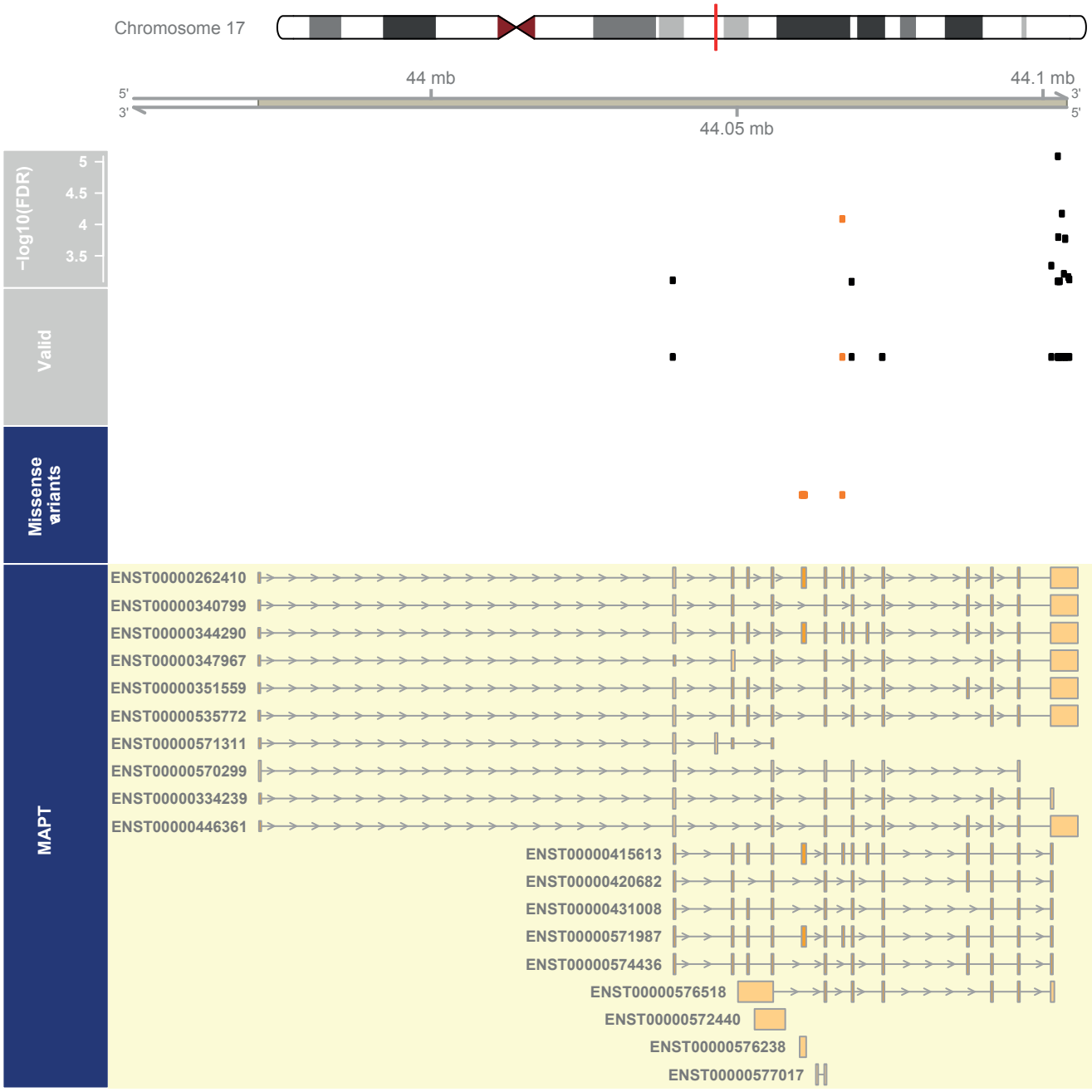

Extended Data Figure 8. ASE sites in *MAPT* in LD with the H1/H2 SNP.

Gene	ColB	ColG	PPI	GWAS	MPD	MLS
ATP13A2					X	X
CCNT2				X		
CD38	X	X		X		
CTSB	X	X	X			
DDRGK1				X		
DGKQ				X		
DJ1					X	
DNAJC13					X	
FBXO7					X	
GALC	X			X		X
GBA			X		X	X
GPNMB	X	X		X		
HSD3B7		X				
IDUA						X
INPP5F			X			
KAT8		X	X	X		
KLHL7		X		X		
LRRK2			X	X	X	
LSM7	X	X		X		
MAPT			X	X		
NCKIPSD	X	X	X	X		
NEK1	X					
NSF			X			
NUCKS1		X		X		
NUPL2	X	X		X		
PDLIM2		X		X		
PM20D1	X					
PRKN					X	
RAB7L1	X	X	X			
SH3GL2			X			
SLC41A1		X		X		
SNCA					X	
SPPL2B	X					
STK39				X		
VAMP4	X	X				
VPS35					X	
WDR6	X	X				
ZNF646				X		

Supplementary Table 1. Complete list of the 38 genes screened in the high content screen. ColB = coloc analysis using Braineac, ColG = coloc analysis using GTEx, WPPINA = weighted protein-protein interaction network; GWAS = genes prioritised in PD-GWAS (Chang *et al*, 2017), MPD = Mendelian genes associated with PD, MLS = Mendelian genes associated with lysosomal storage disorders

eQTL_ dataset	GTEx
sequencing_ method	RNA-seq
gene_ symbol	KAT8
tissue	Brain_Caudate_ basal_ganglia
braineac_ probe_id	NA
nsnps	2499
PPH0	4.89E-10
PPH1	1.76E-07
PPH2	6.76E-04
PPH3	0.242293929
PPH4	0.75702972
PD_top_snp	chr16:31000809
coloc_top_ snp	chr16:31048079
coloc_SNP_ PPH4	0.08637809
coloc_eQTL_ effect_allele	T
coloc_eQTL_ other_allele	C
coloc_eQTL_ beta	-0.358743
coloc_eQTL_ SE	0.0563187
coloc_eQTL_ Freq1	NA
coloc_eQTL_ p_val	3.49E-09
coloc_PD_Al1	C
coloc_PD_Al2	T
coloc_PD_ beta	-0.0739
coloc_PD_ SE	0.0115
coloc_PD_ Freq1	0.5972
coloc_PD_ p_val	1.38E-10

Supplementary Table 2. Results of the Colocalization analysis for KAT8.
PD_top_snp = lead SNP in the PD GWAS, coloc_top snp = Most likely SNP responsible for the colocalization signal, coloc_SNP_PPH4 = posterior probability of coloc top SNP being the true SNP responsible for the colocalization signal.

ID	KAT8	KAT8	KAT8	KAT8	KAT8	KAT8
CHR	16	16	16	16	16	16
P0	31127075	31127075	31127075	31127075	31128984	31127075
P1	31142714	31142714	31142714	31142714	31142714	31142714
HSQ	0.144	0.191	0.121	0.156	0.0641	0.207
BEST.GWAS.ID	rs9938550	rs9938550	rs9938550	rs9938550	rs2305880	rs9938550
BEST.GWAS.Z	-6.82	-6.82	-6.82	-6.82	-6.84	-6.82
EQTL.ID	rs8046707	rs1549293	rs2855475	rs12597511	rs749767	rs4527034
EQTL.R2	0.13718	0.129562	0.227501	0.19827	0.074695	0.00998
EQTL.Z	-4.26	-4.12	-4.58	-4.61	-6.05	-4.23
EQTL.GWAS.Z	6.28455	6.13675	6.1538	6.178	6.06897	6.1724
NSNP	240	240	240	240	248	240
NWGT	3	4	3	1	1	9
MODEL	lasso	lasso	lasso	lasso	lasso	lasso
MODELCV.R2	0.103	0.181407	0.17535	0.17222	0.07213	0.04964
MODELCV.PV	0.000889	1.37E-05	2.91E-05	2.56E-05	3.95E-09	0.0139
TWAS.Z	-6.6932	-6.2068	-6.1876	-6.178	-6.069	-6.04195
TWAS.P	2.18E-11	5.41E-10	6.11E-10	6.49E-10	1.29E-09	1.52E-09
FDR	2.09E-09	4.84E-08	7.15E-08	6.79E-08	4.37E-07	2.36E-07
Region	GTEx.Brain _Cortex	GTEx.Brain_ Nucleus_accumbens _basal_ganglia	GTEx.Brain_ Cerebellar_ Hemisphere	GTEx.Brain_ Frontal_Cortex _BA9	CMC.BRAIN .RNASEQ	GTEx.Brain_ Cerebellum

Supplementary Table 3. Results of the TWAS analysis for *KAT8*.

KAT name	Alternative name(s)
KAT1	HAT1
KAT2A	GCN5
KAT2B	PCAF
KAT3A	CREBBP, CBP
KAT3B	EP300
KAT4	TAF1, TFII250
KAT5	TIP60
KAT6A	MOZ, MYST3
KAT6B	MORF, MYST4
KAT7	HBO1, MYST2
KAT8	MOF, MYST1
KAT9	ELP3
KAT12	GTF3C4, TFIIIC90
KAT13A	NCOA1, SRC1
KAT13B	NCOA3, SRC3, ACTR
KAT13C	NCOA2
KAT13D	CLOCK
	ACAT1
	ATAT1
	ATF2
	BLOC1S1 (GCN5L1)
	NAT10

Supplementary Table 4. Complete list of the 22 KATs screened in the high content screen. (See Fig 3E)

Within each row, compare columns (simple effects within rows)

Number of families	8
Number of comparisons per family	3

Dunnett's multiple comparisons test	Mean Diff.	95.00% CI of diff.	Significant?	Summary	Adjusted P Value
DMSO					
SCR vs. KAT8	0	-14.19 to 14.19	No	ns	>0.9999
SCR vs. KANSL1	0	-14.19 to 14.19	No	ns	>0.9999
SCR vs. PINK1	0	-14.19 to 14.19	No	ns	>0.9999
1 h					
SCR vs. KAT8	21	6.807 to 35.19	Yes	**	0.0017
SCR vs. KANSL1	30	15.81 to 44.19	Yes	****	<0.0001
SCR vs. PINK1	38	23.81 to 52.19	Yes	****	<0.0001
2 h					
SCR vs. KAT8	30	15.81 to 44.19	Yes	****	<0.0001
SCR vs. KANSL1	53	38.81 to 67.19	Yes	****	<0.0001
SCR vs. PINK1	71	56.81 to 85.19	Yes	****	<0.0001
3 h					
SCR vs. KAT8	33	18.81 to 47.19	Yes	****	<0.0001
SCR vs. KANSL1	51	36.81 to 65.19	Yes	****	<0.0001
SCR vs. PINK1	73	58.81 to 87.19	Yes	****	<0.0001
4 h					
SCR vs. KAT8	15	0.8065 to 29.19	Yes	*	0.0355
SCR vs. KANSL1	28	13.81 to 42.19	Yes	****	<0.0001
SCR vs. PINK1	49	34.81 to 63.19	Yes	****	<0.0001
5 h					
SCR vs. KAT8	9	-5.193 to 23.19	No	ns	0.307
SCR vs. KANSL1	21	6.807 to 35.19	Yes	**	0.0017
SCR vs. PINK1	39	24.81 to 53.19	Yes	****	<0.0001
6 h					
SCR vs. KAT8	14	-0.1935 to 28.19	No	ns	0.0542
SCR vs. KANSL1	24	9.807 to 38.19	Yes	***	0.0003
SCR vs. PINK1	42	27.81 to 56.19	Yes	****	<0.0001
7 h					
SCR vs. KAT8	19	4.807 to 33.19	Yes	**	0.0051
SCR vs. KANSL1	23	8.807 to 37.19	Yes	***	0.0005
SCR vs. PINK1	40	25.81 to 54.19	Yes	****	<0.0001

Supplementary Table 5. p-values for Figure 6B.

hetSNP	Sample ID	Read count	Allele	Ens.Alt	Individual ID	Tissue
17:44108355	A653_043	47	A	A	004_06	SNIG
17:44108355	A653_043	20	G	A	004_06	SNIG
17:44108355	A653_441	69	A	A	032_09	PUTM
17:44108355	A653_441	0	G	A	032_09	PUTM
17:44159849	A653_031	2	C	C	024_09	PUTM
17:44159849	A653_031	23	T	C	024_09	PUTM
17:44159849	A653_719	58	C	C	035_09	SNIG
17:44159849	A653_719	26	T	C	035_09	SNIG
17:44248769	A653_093	36	C	C	004_08	SNIG
17:44248769	A653_093	4	T	C	004_08	SNIG
17:44248769	A653_184	30	C	C	013_09	PUTM
17:44248769	A653_184	7	T	C	013_09	PUTM
17:44248769	A653_326	26	C	C	017_09	PUTM
17:44248769	A653_326	3	T	C	017_09	PUTM
17:44248769	A653_617	22	C	C	029_09	SNIG
17:44248769	A653_617	0	T	C	029_09	SNIG
17:44248769	A653_679	23	C	C	030_06	PUTM
17:44248769	A653_679	3	T	C	030_06	PUTM
17:44248769	A653_753	43	C	C	029_09	PUTM
17:44248769	A653_753	10	T	C	029_09	PUTM
17:44248769	A653_794	24	C	C	036_09	SNIG
17:44248769	A653_794	4	T	C	036_09	SNIG
17:44248814	A653_043	10	A	A	004_06	SNIG
17:44248814	A653_043	0	G	A	004_06	SNIG
17:44248814	A653_326	19	A	A	017_09	PUTM
17:44248814	A653_326	3	G	A	017_09	PUTM
17:44248814	A653_617	12	A	A	029_09	SNIG
17:44248814	A653_617	0	G	A	029_09	SNIG
17:44248814	A653_679	19	A	A	030_06	PUTM
17:44248814	A653_679	2	G	A	030_06	PUTM
17:44248814	A653_753	25	A	A	029_09	PUTM
17:44248814	A653_753	5	G	A	029_09	PUTM
17:44248814	A653_950	28	A	A	006_10	SNIG
17:44248814	A653_950	8	G	A	006_10	SNIG

Supplementary Table 6. Summary of the results of ASE analysis across the *KANSL1* gene.

Column name	**Description**
hetSNP	Heterozygous SNP with average read depth >15 across samples
Avg.Reads.all.samples	Average read depth across all samples
min.FDR	Minimum false discovery rate across the samples
Allele1	Allele 1 for the hetSNP
Allele2	Allele 2 for the hetSNP
ens.alt	Ensembl alternate allele
symbol	Gene name obtained using the variant effect predictor tool (VEP)
most.severe.consequence	Most severe of all observed consequence types reported for the hetSNP (VE
ASE	Indicates ASE = 'Y' if min.FDR < 0.05, 'N' if min.FDR >=0.05

The following column details were from obtained from LDProxy (https://ldlink.nci.nih.gov/)

RSID	Identifier for the hetSNP
Alleles	SNP alleles
MAF	Minor allele frequency
Dprime	Indicator of allelic segregation for two genetic variants
R2	Measure of correlation of alleles for two genetic variants.

hetSNP	Sample ID	Read count	Allele	Ens.alt	Individual ID	Tissue
17:44067400	A653_031	18	C	C	024_09	PUTM
17:44067400	A653_031	3	T	C	024_09	PUTM
17:44102689	A653_031	5	C	C	024_09	PUTM
17:44102689	A653_031	21	G	C	024_09	PUTM
17:44103616	A653_031	23	C	T	024_09	PUTM
17:44103616	A653_031	0	T	T	024_09	PUTM
17:44103825	A653_031	11	C	C	024_09	PUTM
17:44103825	A653_031	31	T	C	024_09	PUTM
17:44104509	A653_043	43	C	C	004_06	SNIG
17:44104509	A653_043	82	T	C	004_06	SNIG
17:44102604	A653_056	85	C	C	015_07	PUTM
17:44102604	A653_056	138	T	C	015_07	PUTM
17:44104343	A653_093	84	A	C	004_08	SNIG
17:44104343	A653_093	34	C	C	004_08	SNIG
17:44102689	A653_171	37	C	C	040_08	SNIG
17:44102689	A653_171	87	G	C	040_08	SNIG
17:44039691	A653_177	118	A	G	015_07	SNIG
17:44039691	A653_177	184	G	G	015_07	SNIG
17:44104343	A653_177	35	C	C	015_07	SNIG
17:44104343	A653_177	74	A	C	015_07	SNIG
17:44102689	A653_205	30	C	C	040_08	PUTM
17:44102689	A653_205	64	G	C	040_08	PUTM
17:44102689	A653_225	36	C	C	004_08	PUTM
17:44102689	A653_225	70	G	C	004_08	PUTM
17:44104343	A653_243	37	C	C	021_09	SNIG
17:44104343	A653_243	71	A	C	021_09	SNIG
17:44102689	A653_283	47	C	C	017_09	SNIG
17:44102689	A653_283	90	G	C	017_09	SNIG
17:44102865	A653_283	79	A	C	017_09	SNIG
17:44102865	A653_283	41	C	C	017_09	SNIG
17:44104343	A653_283	42	C	C	017_09	SNIG
17:44104343	A653_283	84	A	C	017_09	SNIG
17:44104509	A653_283	85	T	C	017_09	SNIG
17:44104509	A653_283	43	C	C	017_09	SNIG
17:44067400	A653_288	50	C	C	038_08	PUTM
17:44067400	A653_288	12	T	C	038_08	PUTM
17:44104509	A653_326	73	T	C	017_09	PUTM
17:44104509	A653_326	33	C	C	017_09	PUTM
17:44101563	A653_441	34	C	C	032_09	PUTM

hetSNP	Sample ID	Read count	Allele	Ens.alt	Individual ID	Tissue
17:44101563	A653_441	0	T	C	032_09	PUTM
17:44102638	A653_441	0	A	G	032_09	PUTM
17:44102638	A653_441	197	G	G	032_09	PUTM
17:44102689	A653_441	77	C	C	032_09	PUTM
17:44102689	A653_441	0	G	C	032_09	PUTM
17:44103296	A653_441	112	C	C	032_09	PUTM
17:44103296	A653_441	0	T	C	032_09	PUTM
17:44103825	A653_441	75	C	C	032_09	PUTM
17:44103825	A653_441	0	T	C	032_09	PUTM
17:44103826	A653_441	74	A	A	032_09	PUTM
17:44103826	A653_441	0	G	A	032_09	PUTM
17:44067400	A653_627	9	T	C	033_09	PUTM
17:44067400	A653_627	30	C	C	033_09	PUTM
17:44068924	A653_627	39	A	A	033_09	PUTM
17:44068924	A653_627	72	G	A	033_09	PUTM
17:44102933	A653_627	73	C	C	033_09	PUTM
17:44102933	A653_627	118	T	C	033_09	PUTM
17:44104343	A653_627	68	A	C	033_09	PUTM
17:44104343	A653_627	35	C	C	033_09	PUTM
17:44104509	A653_627	92	T	C	033_09	PUTM
17:44104509	A653_627	53	C	C	033_09	PUTM
17:44102689	A653_643	24	C	C	017_08	PUTM
17:44102689	A653_643	54	G	C	017_08	PUTM
17:44104509	A653_679	11	C	C	030_06	PUTM
17:44104509	A653_679	40	T	C	030_06	PUTM
17:44067400	A653_719	13	T	C	035_09	SNIG
17:44067400	A653_719	51	C	C	035_09	SNIG
17:44102689	A653_719	45	C	C	035_09	SNIG
17:44102689	A653_719	84	G	C	035_09	SNIG
17:44067400	A653_738	23	C	C	036_09	PUTM
17:44067400	A653_738	3	T	C	036_09	PUTM
17:44067400	A653_753	24	C	C	029_09	PUTM
17:44067400	A653_753	6	T	C	029_09	PUTM
17:44101563	A653_763	0	C	C	034_08	PUTM
17:44101563	A653_763	33	T	C	034_08	PUTM
17:44103296	A653_763	0	C	C	034_08	PUTM
17:44103296	A653_763	91	T	C	034_08	PUTM
17:44068924	A653_794	39	A	A	036_09	SNIG
17:44068924	A653_794	73	G	A	036_09	SNIG

Column name	Description
hetSNP	Heterozygous SNP with average read depth >15 across samples
Avg.Reads.all.samples	Average read depth across all samples
min.FDR	Minimum false discovery rate across the samples
Allele1	Allele 1 for the hetSNP
Allele2	Allele 2 for the hetSNP
ens.alt	Ensembl alternate allele
symbol	Gene name obtained using the variant effect predictor tool (VEP)
most.severe.consequen	Most severe of all observed consequence types reported for the hetSNP (VEP)
ASE	Indicates ASE = 'Y' if min.FDR < 0.05, 'N' if min.FDR >=0.05

The following column details were from obtained from LDProxy (https://ldlink.nci.nih.gov/)

RSID	Identifier for the hetSNP
Alleles	SNP alleles
MAF	Minor allele frequency
Dprime	Indicator of allelic segregation for two genetic variants
R2	Measure of correlation of alleles for two genetic variants.

17q21 ORFs	
ACBD4	HEXIM1
ADAM11	HIGD1B
ARHGAP27	KANSL1
ARL17A	KIF18B
ARL17B	LRRC37A
C1QL1	LRRC37A2
CCDC103	MAP3K14
CDC27	MAPT
CRHR1	MYL4
DBF4B	NMT1
DCAKD	NSF
EFTUD2	PLEKHM1
FMNL1	RPRML
GFAP	SPPL2C
GJC1	STH
GOSR2	WNT3

Supplementary Table 8. Complete list of the 32 ORFs in the 17q21 locus screened in the high content screen. (See Fig 9)